https://doi.org/10.5194/essd-2026-798
Preprint. Discussion started: 22 October 2026
© Author(s) 2026. CC BY 4.0 License.



Open Access Earth System Science Data Discussions

High-Resolution Above-Ground Biomass Mapping of the Alps using Satellite Embeddings and GEDI

Anna Candotti[1], Enrico Tomelleri[1, 2]

[1] Faculty of Agricultural, Environmental and Food Sciences, Free University of Bozen-Bolzano, Bolzano, Italy
[2]Competence Centre for Mountain Innovation Ecosystems, Free University of Bozen-Bolzano, Bolzano, Italy

Correspondence to: Anna Candotti (anna.candotti@unibz.it)

Abstract. Accurate estimates of aboveground biomass (AGB) are crucial for understanding terrestrial carbon cycling and informing climate-efficient forest management policies. The diverse topography and altitudinal ranges make the Alps a significant contributor to European carbon stocks. However, existing AGB products often lack sufficient spatial resolution and temporal consistency to capture fine-scale biomass patterns in complex terrain. Here, we present a high resolution (30 m) gridded dataset of AGB (Mg ha^{-1}) for the year 2022 over the Alpine Convention extent. The map was developed by integrating openly accessible GEDI-derived AGB metrics and the Earth Alpha Foundation Satellite Embedding using a random forest regression framework. The model's performance was first evaluated using internal validation against GEDI-derived AGB, showing a high degree of agreement. Independent validation against 2068 National Forest Inventory (NFI) plots confirms the model's ability to generalize across forest types and environmental conditions. Additionally, the dataset's suitability was evaluated by comparing it with existing high-resolution (<= 100 m) AGB estimates, highlighting improved estimates in heterogeneous mountainous terrain. The outputs were further used to discuss the spatial distribution of AGB across the region, highlighting the roles of climatic patterns, elevation, and forest composition in shaping AGB distributions. The dataset provides a high-resolution, spatially explicit representation of AGB across the Alpine region and is a valuable resource for regional carbon accounting, forest management, and environmental modeling. The dataset is available at: https://doi.org/10.5281/zenodo.23073080 (Candotti and Tomelleri, 2026).

1 Introduction

Terrestrial living biomass constitutes roughly 30% of the Earth's total carbon storage (Batjes 1996). The sequestration of carbon in vegetation makes management of forest biomass relevant to the challenge of limiting global warming to 2 °C, an internationally agreed target (UNFCCC 2015). Vegetation biomass also has a pivotal role in influencing climate by modifying water and energy exchanges with the atmosphere (Ellison et al., 2017), in providing habitat for numerous species as well as resources for humans. Disturbances (including human, wind, insects and fire) lead to loss of biomass and, in the case of decomposition, can result in carbon dioxide and other greenhouse gas (GHG) emissions (Herold et al., 2019). In addition to disturbances, the ability to store carbon further depends on environmental conditions, topography, species composition and

https://doi.org/10.5194/essd-2026-798
Preprint. Discussion started: 22 October 2026
© Author(s) 2026. CC BY 4.0 License.



age (Pan et al., 2013). Spatially accurate estimations are thus crucial for understanding the carbon cycle, for monitoring ecosystem health as well as for mitigation and adaptation actions (Harris et al., 2021).

Total plant biomass comprises both aboveground biomass (AGB) and belowground biomass, such as roots. Traditional methods for measuring AGB rely on field-based approaches, either through destructive sampling or through allometric models that rely on tree metrics such as height and diameter at breast height (DBH). National Forest Inventories (NFIs) provide essential field-based reference data, which enables the calibration of biomass models used in carbon storage assessments (Tomppo et al., 2009). Estimating biomass baselines and increases in carbon storage over time, however, is hampered by the data periodicity in these initiatives, which can exceed five to ten years in most countries of the northern hemisphere (Bontemps and Bouriaud, 2024).

From a space-based perspective, both optical (e.g., Landsat, Moderate Resolution Image Spectroradiometer (MODIS)) and RADAR (e.g., ALOS PALSAR, ENVISAT ASAR) data have been used for AGB mapping. RADAR-based measurements, however, have greater sensitivity to forest biomass than optical systems, especially at longer wavelengths. The main limitation of optical products in estimating AGB is related to its quick saturation over densely vegetated areas (saturation at around 100 Mg ha^{-1}) (Brandt et al., 2018). RADAR-based estimates have shown great potential for biomass estimates, in particular, when combined with Light Detection and Ranging (LiDAR as for example ICESat, GLAS)(Saatchi et al., 2011; Santoro et al., 2021). The emergence of large-scale and multi-temporal satellite imagery enabled the creation of the first wall-to-wall AGB datasets in the early 2010s (Baccini et al., 2012; Saatchi et al., 2011).

When extensive ground-truth data is unavailable, existing wall-to-wall AGB maps (Fan et al., 2019) and spatially dense spaceborne LiDAR estimates (Shendryk, 2022) offer practical alternatives for training retrieval models. Compared to forest-restricted measurements in NFI data, LiDAR from NASA's Global Ecosystem Dynamics Investigation (GEDI) broads the sampling range to include short-stature vegetation, savanna and shrubland ecosystems (Dubayah et al., 2020). Model training can account for spatial variability in how the Earth Observation (EO) signals respond to AGB, but it may propagate biases in the map-based AGB values into the derived AGB retrieval model (Salazar-Neira et al., 2023).

The pixel size is still limited in global biomass products varying between 100 meters and several kilometers (Santoro et al., 2021). This represents a particular challenge in strongly heterogeneous landscapes, such as in complex terrain where elevation drives the spatial variability of AGB, as well as in areas characterized by frequent changes induced by forest disturbances or land use changes which can occur at finer spatial scales. Moreover, biomass products obtained from RADAR data can be prone to errors on steep slopes (Klaas-Witt and Emeis, 2022). These factors lead to significant disagreements across products that also reduce their value for estimating carbon stocks and their temporal dynamics in global and regional applications. In addition, because these maps exhibit distinct individual error properties, comparing maps from different epochs remains an unreliable method for analyzing biomass change (Araza et al., 2022).

As climate mitigation strategies are often implemented at the scale of regional administrative units, reliable biomass estimates at high spatial resolutions are required. Studies have started to address this by spatially extrapolating GEDI height measurements with ancillary continuous satellite data such as Sentinel-1 and Sentinel-2 (Schwartz et al., 2023) or ALOS

https://doi.org/10.5194/essd-2026-798
Preprint. Discussion started: 22 October 2026
© Author(s) 2026. CC BY 4.0 License.



PALSAR-2 RADAR data and topographic variables (He et al., 2026) to create AGB maps at spatial resolutions < = 30 m at the country level. The creation of such products is particularly relevant in alpine regions, where terrain complexity and fragmented land use shape the spatial distribution of biomass.

In this work, we present a high spatial resolution (30 m) AGB map over the area that the Alpine Convention agreement defines as the Alps' extent. Our objective addresses fundamental uncertainties in the spatial distribution of AGB in complex terrain and the lack of wall-to-wall biomass estimates across the entire alpine region, aside from continental or global products. Furthermore, we investigate the use of Satellite Embeddings to test if these multi-modal representations can overcome the intrinsic shortcomings of existing remote sensing products that rely on a single data source. The resulting product aims to capture the small-scale terrain features of the region to be used for local-scale biomass assessments in complex terrain. This work also aims to compare existing biomass products to assess their accuracy and consistency in mountain areas.

The gridded dataset is computed by integrating GEDI-derived AGB and Alpha Earth Foundation (AEF) Satellite Embeddings for the year 2022. The methodology per se is transferable as it entirely relies on open-source global data products. In Sect. 2 the data collection, processing and validation of the maps are explained, while in sect. 3 the results are discussed on the basis of cross-validations with NFI data and existing AGB products. The spatial distribution of AGB is discussed in relation to topography and climatic patterns that characterize the mountainous terrain of the alpine area. Potential, limitations and use cases are suggested in sect. 4.

2 Datasets and methods

2.1 Study area

With elevations ranging from close to sea level to 4809 meters above sea level (m a.s.l.), the European Alps are a mountain range in Central Europe that includes portions of France, northern Italy, Switzerland, southern Germany, Austria, and Slovenia. We took into account the 190,000 km ² area that the Alpine agreement defines as the Alps' extent (Fig. 1). The climate zones found in the Alps range from Alpine to Mediterranean and from temperate-Atlantic to temperate-continental. With the upper tree-line between 1800 and 2400 m a.s.l., forests cover about 57% of the Alps. Broadleaved trees like European beech (*Fagus sylvatica* L.) dominate forests at lower elevations, while at higher elevations conifers such as Norway spruce (*Picea abies* (L.) Karst), European Larch (*Larix decidua* L.), and various pine species (mainly *Pinus cembra* L. and *P. mugo* Turra) are dominant.

https://doi.org/10.5194/essd-2026-798
Preprint. Discussion started: 22 October 2026
© Author(s) 2026. CC BY 4.0 License.

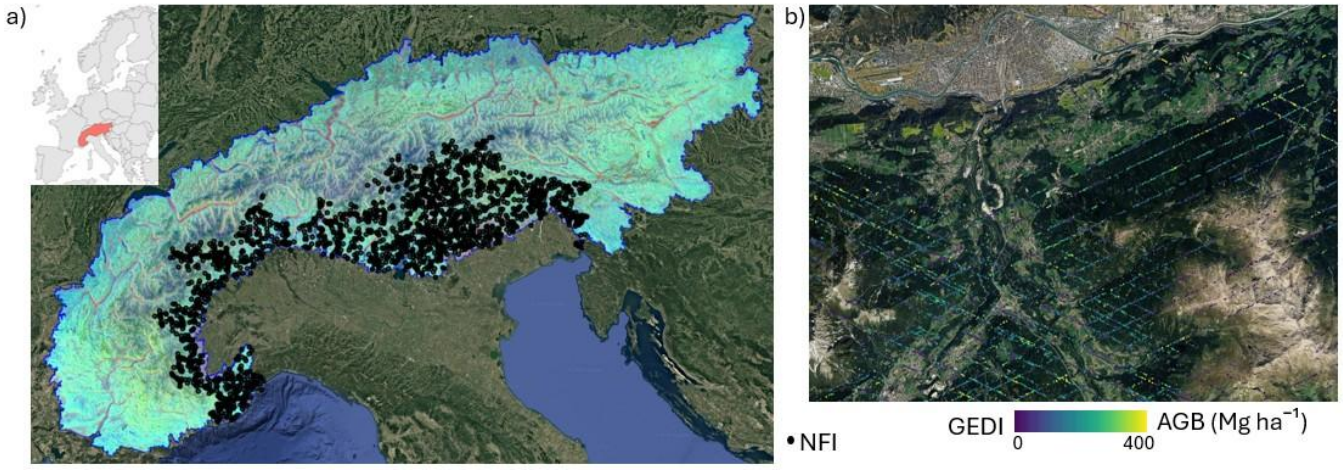


Figure 1: a) Alpha Earth Satellite embeddings over the alpine convention regional extent (bands used for visualization: B02, B08, B33). Forested areas are depicted in yellow (high forest cover density) and turquoise (lower forest cover density), mountain valleys in red and non-vegetative surfaces in grey. The distribution of National Forest Inventory (NFI) plots used for independent above ground biomass (AGB) validation are shown in black. b) example of GEDI footprint and pixel based AGB estimates (Mg ha^{-1}) used for training, shown on a cut-out southern of the city of Innsbruck (Austria).

2.2 Alpha Earth Foundation Satellite Embeddings

The AEF initial collection, spanning the years 2017–2024, provides 64-dimensional, unitless embeddings that encode temporal and spatial relationships among key planetary variables derived from EO data (Brown et al., 2025). An embedding is a numerical vector that captures the salient characteristics of an observation in a learned latent space, where observations with similar properties are positioned closer together. The embedding model learns this latent representation by transforming the original high-dimensional input data into a feature space that preserves meaningful relationships among observations. The embeddings integrate information from multiple geospatial sources, including optical and thermal imagery (Sentinel-2 and Landsat), RADAR (Sentinel-1 and ALOS PALSAR-2), spaceborne LiDAR (GEDI), land-cover datasets (LCMAP and LUCAS), digital elevation models (Copernicus GLO-30), environmental datasets (ERA5-Land and GRACE), and descriptive text (e.g., NLCD and Wikipedia). They are provided at a 10 m spatial resolution, enabling the characterization of fine-scale land-cover transitions. Each embedding encodes the annual spatiotemporal trajectory of a pixel. We selected the 2022 embeddings because they benefit from the upgraded GEDI geolocation and footprint-placement algorithms and provide the most complete single-year GEDI coverage for the Alpine region prior to the mission interruption.

2.3 Above-ground biomass (AGB) estimates from GEDI

The GEDI instrument, attached to the International Space Station (ISS), collects data globally between 51.6° N and 51.6° S latitudes at 25-m spatial resolution. The GEDI instrument collects LiDAR measurements along a total of eight beam ground transects, which instantaneously sample eight ~ 25 m footprints spaced approximately every 60 m along-track and 600-meter

https://doi.org/10.5194/essd-2026-798
Preprint. Discussion started: 22 October 2026
© Author(s) 2026. CC BY 4.0 License.



across-track. In addition to the full waveform data, estimates of AGB with the GEDI L4A raster product are provided. In this product, predictions of the aboveground biomass density (Mg ha^{-1}) and estimates of the prediction standard error within each sampled geolocated laser footprint are available. Height metrics from simulated waveforms associated with field estimates of AGB from multiple regions and plant functional types (PFTs) were compiled to generate a calibration dataset for models representing the combinations of world regions and PFTs (i.e., deciduous broadleaf trees, evergreen broadleaf trees, evergreen needleleaf trees, deciduous needleleaf trees, and the combination of grasslands, shrubs, and woodlands). The algorithm uses GEDI02_A relative height metrics and 13 linear models to predict AGB in 32 combinations of plant functional type and world region within the observation limits of the ISS. GEDI04_A models for the release 1 and release 2 data products were developed using 8,587 quality-filtered simulated GEDI waveforms associated with field estimates of AGB in 21 countries (Kellner et al., 2023). Alpine countries were excluded from the 21 calibration countries for GEDI04_A Release 1 and 2 because their specific co-located field plots and airborne lidar datasets were not integrated into the foundational database; instead, the algorithm matched Alpine plant functional types to equivalent models optimized using data from calibrated European nations. The raster images are organized as monthly composites of individual orbits in the corresponding month. GEDI's waveform models often overestimate AGB in sparse or low-biomass areas (under 100 Mg ha^{-}) and underestimate it in dense, multi-layered or high-biomass forests (over 200 Mg ha^{-}) with reported standard errors < 30 Mg ha^{-} (Dubayah et al., 2022).

Following the GEDI Level 2 User Guide (Beck et al., 2021), we removed all measurements not meeting quality requirement (l4_quality_flag = 0 and degrade_flag > 0), with high relative error ('agbd_se' / 'agbd' > 50%). We also removed measurements on slopes > 30% based on the Copernicus GLO-30 Digital Elevation Mode (DEM), as they are prone to error.

Considering the horizontal accuracy of +/- 9 m of GEDI data, before sampling pixels to train the regression model, a pixel variance analysis was conducted over the study area. To ensure the spatial representativeness of the GEDI training points and mitigate sub-pixel variability or edge effects related to land cover changes, pixels falling on heterogeneous areas were discarded from the training sample. Pixel variance was assessed in a moving window of 3x3 by computing the Normalized Difference Vegetation Index (NDVI) at 10-m spatial resolution from Sentinel-2 (averaged band values for the year 2022) (Fig. S1). A standard deviation threshold of 0.04 was set, above which pixels were discarded. A class band from the GEDI mask was created and we used stratified sampling to ensure we sampled from the non-masked pixels, however not using a land-cover specific filter on the GEDI footprints. This yielded between 400 and 900 valid GEDI observations per tile (Fig. S2).

2.4 Above-ground biomass (AGB) prediction and validation

We calibrated a model with the embeddings and GEDI data for AGB using random forest (RF) regression. RF has been shown to be capable of modeling large numbers of non-independent or non-linearly separable predictor variables and is less sensitive to noise and feature selection. These properties make RF particularly well suited for monitoring complex ecosystems using diverse remote sensing variables, including forest height, biomass estimation, and forest classification (Belgiu and Drăgu, 2016). Satellite embedding bands (10x10m native pixel size) were used as predictors and GEDI AGB values (25-m native spatial resolution) as the predicted variable in a regression model. We resampled and reprojected the inputs to a pixel size of

https://doi.org/10.5194/essd-2026-798
Preprint. Discussion started: 22 October 2026
© Author(s) 2026. CC BY 4.0 License.


30x30 m using block aggregation. The alpine extent was divided into tiles of 100x100 km to overcome computation limits. To prevent overfitting, the filtered GEDI dataset was partitioned into independent subsets using a randomized split ratio of 70% (training) and 30% (test). To improve computational efficiency and generalization performance, the optimal model configuration, defined by the highest prediction accuracy, was found to be numberOfTrees = 150 and bagFraction = 0.6. Restricting the predictor set to the most influential variables (Fig. S3) based on variable importance scores did not yield significant changes in predictive accuracy. Consequently, all 64 embeddings were retained for the final model.

A framework for tracking uncertainty propagation was deployed generating a pixel-level uncertainty layer. The absolute total uncertainty (σtotal) (Eq. 1) for each 30 m grid cell was mathematically quantified through Gaussian error propagation using three independent, mutually un-correlated variance components:

$$\sigma_{total} = \sqrt{\sigma^2_{GEDI_{SE}} + \sigma^2_{RF_{SE}} + RMSE^2} \quad (1)$$

where σGEDI_SE denotes the aggregated data-level observation uncertainty, quantified as the footprint-level prediction standard error of the GEDI Level 4A Raster Aboveground Biomass Density product (USFS LARSE/GEDI/GEDI04_A_002_MONTHLY); σRF_SE is the local model structural uncertainty computed as the pixel-wise standard deviation across the predictions of the 150 individual Random Forest regression trees; and RMSE capturing residual sub-pixel resampling artifacts induced by the 10 m to 30 m Satellite Embedding aggregation, spatial geolocation mismatches between GEDI footprints and raster pixels, and structural sub-pixel heterogeneity, empirically derived from the independent validation test split empirically from the independent 30% out-of-sample validation partition per tile. Relative uncertainty (% σtotal) was subsequently mapped by normalizing the absolute uncertainty against the local AGB prediction. The Google Earth Engine (GEE) Cloud computing platform was used for all calculations.

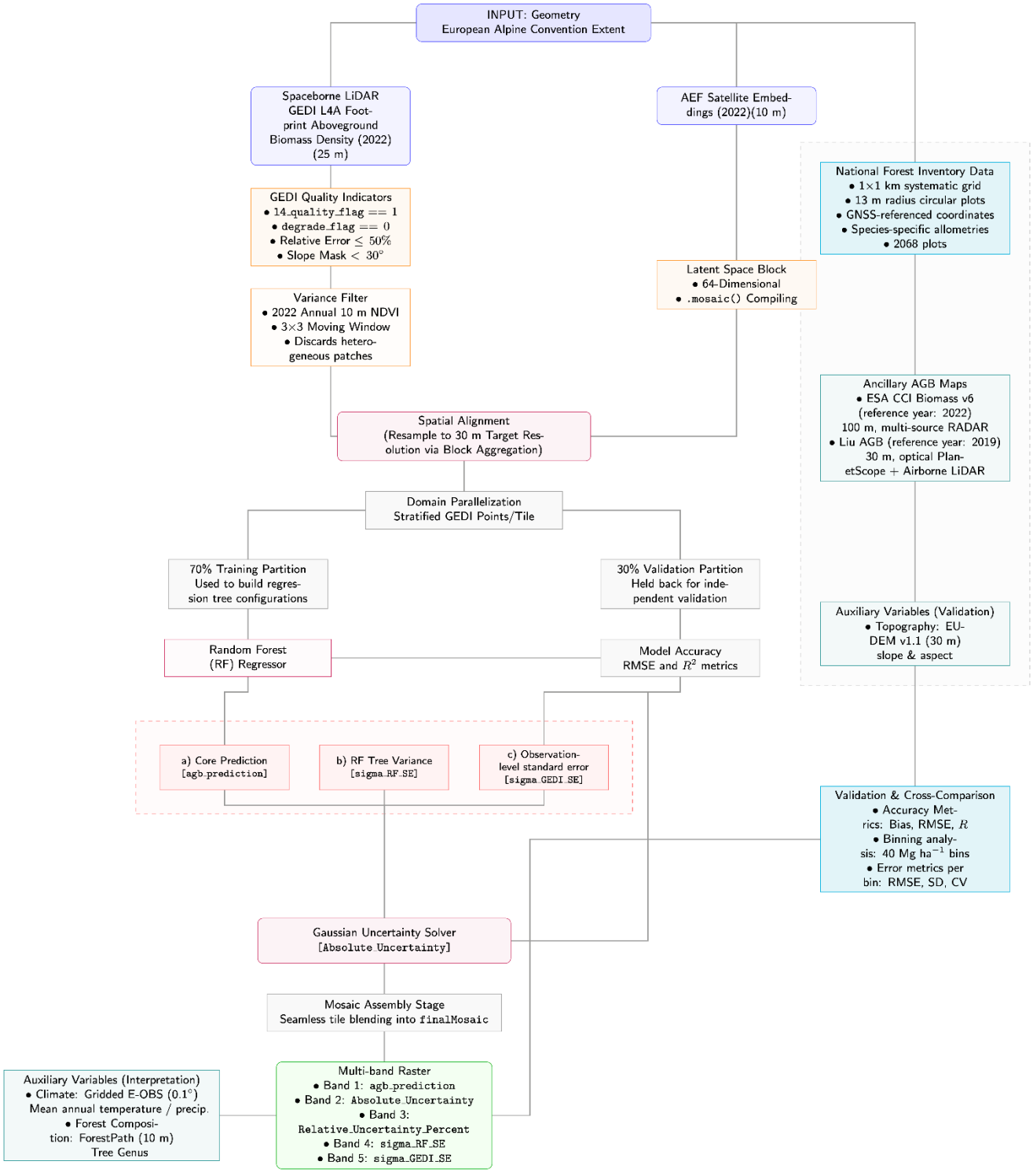
To verify the mathematical validity of the parametric Gaussian distribution assumptions in this complex mountain terrain, an *a posteriori* non-parametric validation check was executed. Using the out-of-sample residual pool from all validation segments, a non-parametric Monte Carlo bootstrapping simulation (n =10 000 iterations) was performed. The empirical prediction intervals generated via Monte Carlo sampling were statistically compared against the theoretical parametric boundaries to evaluate potential structural biases, right-skewness, or heavy-tail anomalies induced by topographic distortions.

The sequence of processing steps is represented in a flow diagram in Fig. 2.

https://doi.org/10.5194/essd-2026-798
Preprint. Discussion started: 22 October 2026
© Author(s) 2026. CC BY 4.0 License.



Open Access Earth System Science Data Discussions



https://doi.org/10.5194/essd-2026-798
Preprint. Discussion started: 22 October 2026
© Author(s) 2026. CC BY 4.0 License.



Figure 2: Methodological workflow for Aboveground Biomass (AGB) prediction and uncertainty characterization. The pipeline details the integration of spaceborne LiDAR (GEDI L4A) and Satellite Embeddings within the European Alpine Convention extent. Processes include input quality filtering, domain parallelization, Random Forest regressor calibration, and a Gaussian Uncertainty Solver used to characterize error metrics within a unified uncertainty framework. Independent validation is conducted using National Forest Inventory (NFI) plot data, comparative AGB maps as well as auxiliary variables for validation (Topography) or interpretation of outputs (Climate, Forest Composition).

2.5 AGB from the National Forest Inventory (NFI)

To assess the accuracy of the AGB maps, forest field data collected by the Italian NFI was used. The NFI employes a systematic, unaligned sampling design based on a 1 km x 1 km grid (Fattorini et al., 2006). Locations are stratified by administrative regions (NUTS2 level) and forest types. At these locations, quantitative data are collected within 13-meter radius circular plots (including tree species, diameter at breast height (DBH), and tree height), which were used to calculate AGB for each callipered tree using national species-specific allometric models (Tabacchi et al., 2011). The spatial distribution of the plots was designed to cover different tree species and elevation gradients. The spatial sampling units (plots) are referenced with global navigation satellite system (GNSS) coordinates, ensuring precise alignment with the high-resolution imagery described in Section 2.8. Plot-level AGB was derived by aggregating tree-level dry weight of total above-ground biomass of the living tree. 2068 points falling within the Alpine Convention extent were selected in this study. Field measurements for the third Italian National Forest Inventory (INFC2015) were conducted between 2017 and 2020. NFI plots from a single nation were selected to ensure methodological consistency in field measurements and AGB estimation. Furthermore, they encompass altitudinal and climatic gradients as well as forest species that are representative of the ecological conditions across the entire perimeter of the Alpine Convention.

2.6 Ancillary AGB datasets

The ESA CCI Forest Above Ground Biomass v.6 (hereafter CCI Biomass) consists of annual, global maps of AGB with pixel size of 1 hectare for the years 2007, 2010, 2015 and 2022. The product's estimates were derived from a combination of Earth observation data, depending on the year, obtained from the Copernicus Sentinel-1 mission, Envisat's ASAR (Advanced Synthetic Aperture RADAR) instrument, and JAXA's Advanced Land Observing Satellite (ALOS-1 and ALOS-2), along with additional information from other Earth observation sources. For this study, we considered the AGB dataset for 2022.

The AGB product for Europe at 30 m spatial resolution by Liu et al. (2023) was created by training deep learning models with airborne LiDAR to predict tree height and tree cover from Planet Scope optical images from 2019 at 3 m spatial resolution. Canopy heights were then used to convert tree cover and height into AGB maps by establishing allometric relationships with the use of forest inventory data.

https://doi.org/10.5194/essd-2026-798
Preprint. Discussion started: 22 October 2026
© Author(s) 2026. CC BY 4.0 License.



2.7 AGB validation and cross-comparison

To measure the goodness the calibrations and validations, we computed the bias, the Root Mean Square Error (RMSE), and the Pearson's correlation (R) between predicted and GEDI-derived AGB. RMSE was also separately calculated for each tile (Fig. S6).

Predicted AGB from this study, GEDI-derived AGB and estimates from two maps described in 2.6, based on remote sensing data close in time to the data used here and similar spatial resolution (<100 m), were used to quantify the agreement with NFI-based AGB. The assessment was based on each product's original spatial resolution and by stratifying the reference NFI AGB into contiguous ranges of values. The comparison was conducted per biomass class using bins of 40 Mg ha^{-1} defined with regard to the NFI plot values. The selected range allowed to have a sufficient number of reference data within each NFI reference range. A spatial variance analysis was conducted within a 100 m radius buffer around each NFI plot center to quantify surrounding landscape heterogeneity and evaluate its relationship with plot-to-pixel AGB prediction errors (Fig. S4 and S5).

In addition to overall bias, RMSE and R, the mean, standard deviation (SD), SD of the errors, and the Coefficient of Variation (CV) of the error defined as the ratio between SD of the errors and bias were calculated following Rodriguez-Veiga et al., (2019). When analysing specific forest types or biomass levels, evaluating the error structure by biomass bins is essential. This is because a map can be unbiased overall, yet still exhibit significant and varying biases within specific biomass ranges (Avitabile and Camia, 2018). Because the true value remains unknown, all error metrics and inter-product differences in this manuscript should be interpreted as variations within an uncertainty framework rather than as absolute errors.

2.8 Auxiliary datasets

Auxiliary datasets were used to understand the signatures of our AGB product as well as detect structural deficiencies in the other products. To comprehensively assess how topography affects AGB estimates, we compared our predictions with those from ESA CCI and Liu stratified by terrain slope and aspect. For this analysis, all maps were first harmonized to the same pixel size of 100x100m. A Digital Terrain Model (DTM) (EU-DEM v1.1, 2016) of 30 m spatial resolution was retrieved to calculate slope and aspect. After resampling to a 100x100 m pixel size by using bilinear interpolation, the calculation of slope and aspect was performed by using the terrain function of the *terra* package in R. Bilinear interpolation was used because it preserves positional geometric trends across the continuous terrain surface, whereas simple block averaging flattens distinct landscape features into artificial steps. Slope was binned into four classes by slope angles contained in the ranges of i) 0-20, ii) 20-40, iii) 40-60, iv) 60-80°. Aspect values were reclassified into four classes as follows: North (315°–45°), East (45°–135°), South (135°–225°), and West (225°–315°).

Additionally, for a comparative analysis of the products' AGB distributions at their original pixel size, but at larger scale (landscape), three cut-out areas representing diverse forest types and topographies were chosen. Specifically, scene i) features

https://doi.org/10.5194/essd-2026-798
Preprint. Discussion started: 22 October 2026
© Author(s) 2026. CC BY 4.0 License.


pure Norway spruce stands on moderate to steep exposed slopes (20–60°), scene ii) comprises montane European beech forests with mixed Norway spruce patches on steep terrain (20–70°), and scene iii) captures oak-dominated with sparse pine trees in a hilly Mediterranean environment. These areas were chosen as they are representative for the broader Alpine space in terms of commonly found forest compositions and topographic gradients. Areal images (Esri) of the three scenes are shown in Fig. S7, S8, S9.

The DTM was additionally used to assess distributions of AGB by altitudinal belts (<500; 501-1000; 1001-1500; 1501-2000; 2001-2500 m a.s.l.) (Fig. A1).

Long-term (1950-2024) mean annual temperature (°C) (MAT) and precipitation (mm year^{-1}) (MAP) were derived from gridded (0.1°) E-OBS climate data (10.24381/cds.151d3ec6) (Cornes et al., 2018) (Fig. A3) and masked to the Alpine Convention perimeter. Predicted AGB was averaged to 10x10 km and was plotted as a function of MAT and MAP in 10x10 km bins (Fig. S10).

The Forest Path European tree genus map available at a 10-m resolution for the year 2020 was used to extract distributions of AGB by tree genus at a common pixel size of 30 m (Fig. A3). The tree genus map data were derived from Sentinel-1 and Sentinel-2 satellite data and are stored in a public repository (10.5281/zenodo.13341104). The map distinguishes seven *genus* classes (Larix, Picea, Pinus, Fagus, Quercus, other needleleaf, other broadleaf). The map was generated using a CatBoost model trained on forest plot inventories, citizen science observations, orthophoto interpretation, and LUCAS data, with additional features from DEM and climate datasets. Labels were filtered and aggregated to genus level to reduce noise (De Keersmaecker et al., 2024).

3 Results

The AGB distribution was found to be spatially heterogeneous with the highest AGB values being concentrated in the eastern regions and lower values in the south-western regions (Fig. 3). Large spatial variability of AGB was observed over the entire territory. AGB ranged between 30 Mg ha^{-1} (minimum) and 470 Mg ha^{-1} (maximum). The first quantile was found within 88 Mg ha^{-1}, the median at 129 Mg ha^{-1}, a mean of 135 Mg ha^{-1} and the third quantile at 172 Mg ha^{-1}. A carbon stock of 3 Pg was estimated across the alpine area.

https://doi.org/10.5194/essd-2026-798
Preprint. Discussion started: 22 October 2026
© Author(s) 2026. CC BY 4.0 License.

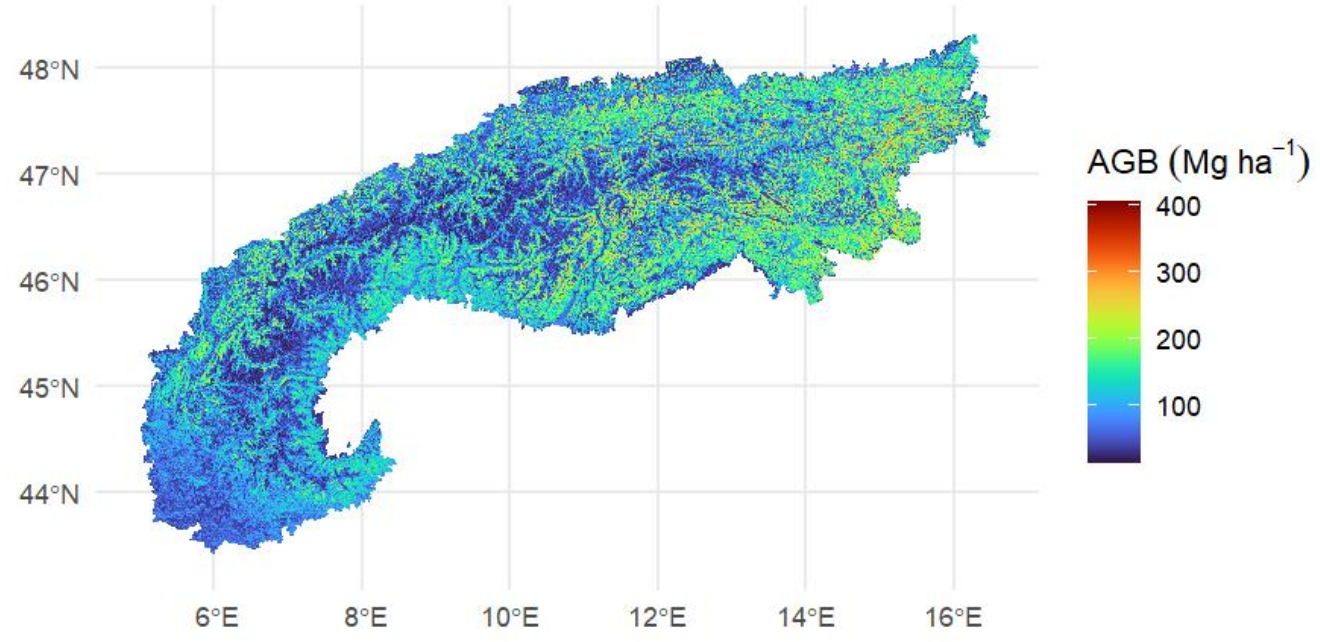


Figure 3: Predicted above-ground biomass (AGB) (Mg ha^{-1}) at 30 m spatial resolution over the Alpine Convention extent. Resampled to 500805 cells for visualization.

The model validation statistics indicate a strong correlation between the estimated AGB and the GEDI observations, suggesting that the RF model generalizes well to the data. However, it tends to slightly overestimate low biomass and underestimate high biomass values (Fig. 4). This tendency can be attributed to the limitations of the RF algorithm in not being able to correctly estimate extremes because of optimizations towards the mean values (Baccini et al., 2008) The underestimation of high AGB (> Mg ha^{-1}) is also a well-known bias in RADAR-derived products (Santoro et al., 2021) and to an even higher degree in optical data. This can be explained by a lack of sensitivity using either the RADAR backscatter or reflectance to biomass in the upper ranges of AGB paired with an incorrect model fit. Predictions based on Satellite Embeddings revealed similar limitations linked to possible saturation for AGB > 400 Mg ha^{-1}. This could be additionally affected by too few observations in the very high AGB ranges in the set of data points used to calibrate the RF model.

https://doi.org/10.5194/essd-2026-798
Preprint. Discussion started: 22 October 2026
© Author(s) 2026. CC BY 4.0 License.

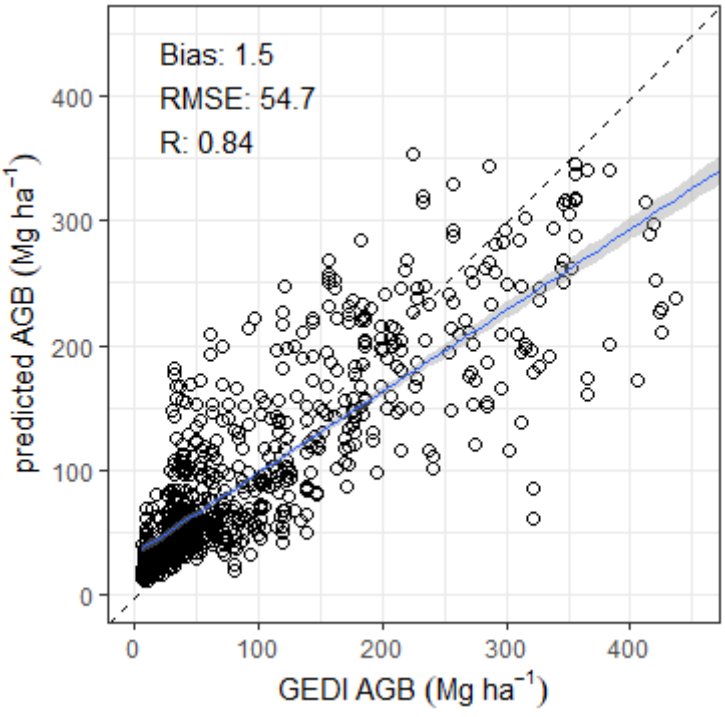
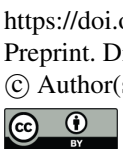


Figure 4: Model validation between GEDI-derived Above-Ground Biomass (AGB) and predicted AGB (Mg ha⁻¹). The dashed line corresponds to the y = x line, while the blue line represents a linear regression model fit with the confidence interval displayed in gray. Global performance metrics (Bias, Root Mean Squared Error (RMSE) (Mg ha⁻¹) and the R metric) are provided in the upper-left annotation box.

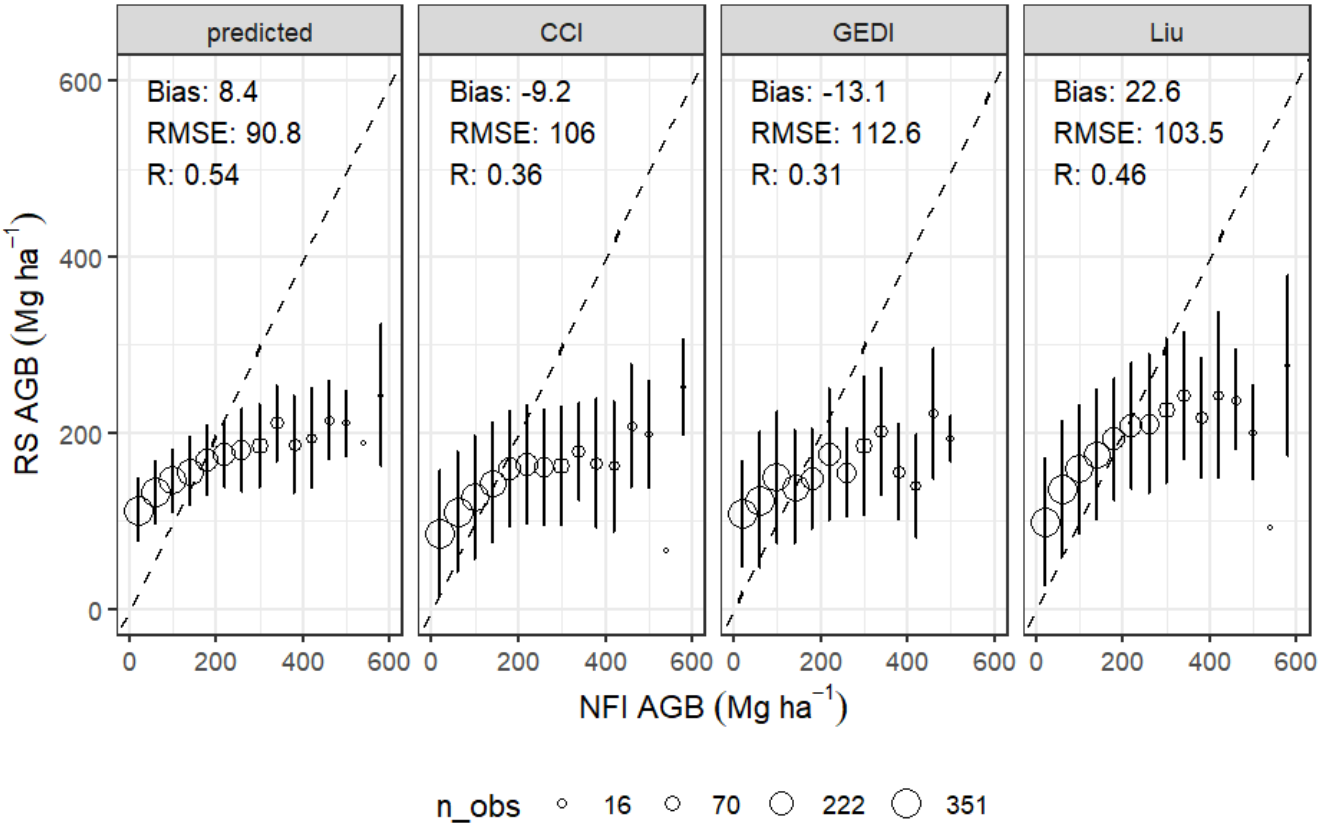
With respect to AGB from NFI data, the predicted AGB values' ranges are lower with maxima slightly above 300 Mg ha⁻¹, while NFI derived estimates reached up to 600 Mg ha⁻¹, revealing larger discrepancy (Fig. 5). Despite this, AGB from independent NFI data showed a moderate correlation with predicted AGB and other products. The accuracy analysis revealed several commonalities among different products. All remote sensing products over-estimate AGB for the lower AGB ranges and under-estimate upper ranges. While this is a well-known problem for earth observations across biomes (Rodríguez-Veiga et al., (2019), higher discrepancies with respect to previous studies were found in this study across all products, especially at AGB ranges > 300 Mg ha⁻¹. The obtained results thus suggest overall higher bias (mean = 101 Mg ha⁻¹) and RMSE (mean = 119 Mg ha⁻¹), when averaging across all AGB ranges.

For our product, RMSE was lower at all AGB ranges up to 280 Mg ha⁻¹ compared to the other products (Fig. 6). At higher AGB ranges, RMSE was found to increase linearly for all products. The SD of errors was consistently lower in our product. All remote sensing products were dominated more by bias than by random error across all AGB ranges, showing similar

https://doi.org/10.5194/essd-2026-798
Preprint. Discussion started: 22 October 2026
© Author(s) 2026. CC BY 4.0 License.



310 degrees of overestimation bias at AGB ranges < 200 Mg ha^{-1} for CCI, GEDI and Liu and to a less extent for our product (Fig. 5). For AGB ranges > 200 Mg ha^{-1} the underestimation bias was found to be similar among CCI, GEDI and our product, while Liu showed slightly higher underestimations (Fig. 6).



315 **Figure 5: Scatterplots of average and standard deviation of Above-Ground Biomass (AGB) from Remote Sensing (RS) products versus reference AGB per National Forest Inventory (NFI) reference range. The dashed line corresponds to the y = x line. If the error bars do not overlap the y = x line then bias is the dominant error in that AGB range. Circles show the mean Above-Ground Biomass (AGB) of different products (predicted from this study, CCI Biomass, Liu and GEDI) in each 40 Mg ha^{-1} wide interval of field inventory (NFI) AGB values. Circle sizes are dynamically scaled** 320 **according to the quartiles (25%, 50%, 75%, and 100%) of the number of observations (n_obs) per bin. Global performance metrics (Bias, Root Mean Squared Error (RMSE) and the R metric) were calculated across the entire un-binned dataset and are provided in the upper-left annotation box. Error metrics and inter-product differences should be interpreted as variations within an uncertainty framework rather than as absolute errors.**

https://doi.org/10.5194/essd-2026-798
Preprint. Discussion started: 22 October 2026
© Author(s) 2026. CC BY 4.0 License.

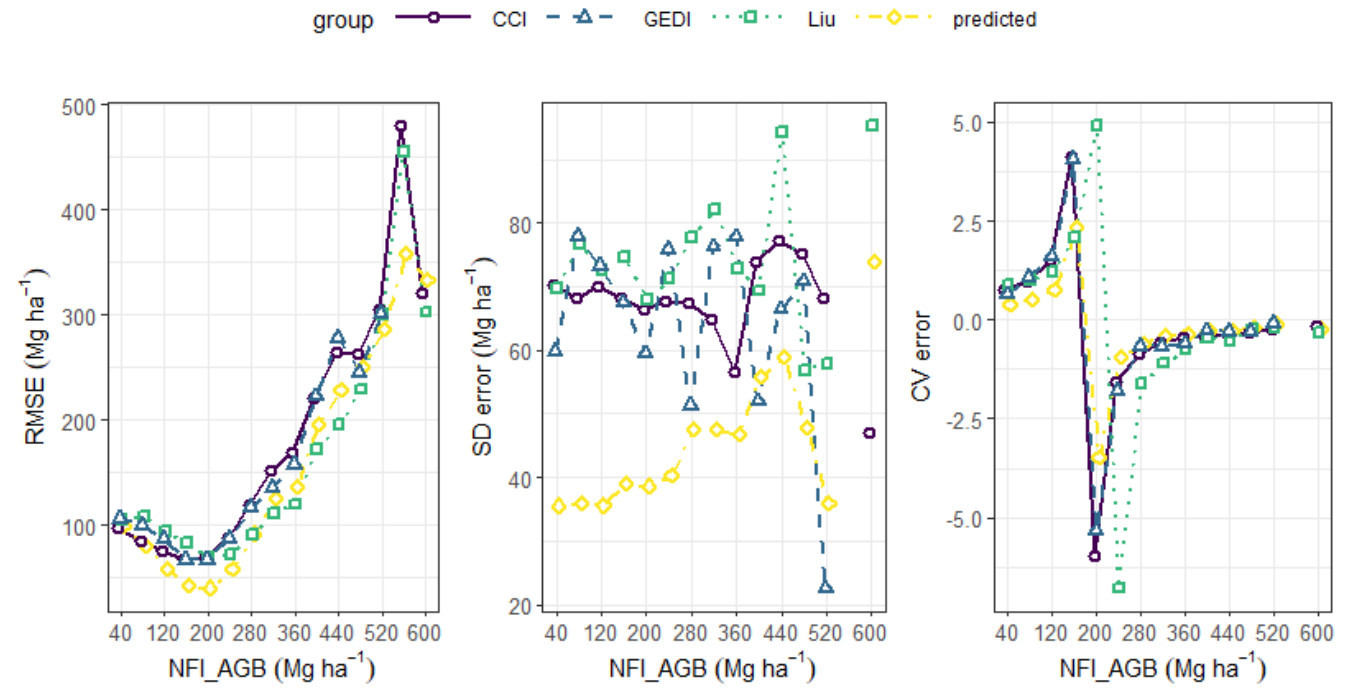


Figure 6: Root Mean Squared Error (RMSE), Standard Deviation (SD) of errors, Coefficient of Variation (CV) of the error, grouped by Above-Ground Biomass (AGB) product from Earth Observations per National Forest Inventory (NFI) reference ranges of 40 Mg ha⁻¹ each. Error metrics and inter-product differences should be interpreted as variations within an uncertainty framework rather than as absolute errors.

Predominant negative differences were found in the CCI product compared to predicted values of this study at high AGB ranges (> 250 Mg ha⁻¹) on steep slopes (40-80°) (Fig. 7). This could be explained by biases in the RADAR-based estimates in complex terrain due to their sensitivity to steep slopes and errors during pre-processing. The Liu optical product was affected by negative differences to a less extent on increasing slope steepness.

In relation to aspect, a negative difference was found in the CCI product on north and eastern facing slopes (Fig. 8). This could be explained by the look geometry of the RADAR sensors (Santoro and Cartus, 2019). As CCI Biomass combines ascending and descending data from Sentinel-1 and ascending data from ALOS-2 and ALOS-2 being predominant, northeast slopes result in shadow, possibly explaining AGB underestimation bias. For the Liu product bias found in the AGB ranges > 300 Mg ha⁻¹ on northern and western facing slopes. PlanetScope CubeSats operate in sun-synchronous orbits with descending nodes designed to pass overhead during mid-to-late local morning. At this time of day, the sun is positioned in the southeastern sky (low eastern solar azimuth angle). Illumination asymmetry can be generated on north-western slopes that receive oblique, grazing sunlight during the morning pass. This causes extensive intra-crown self-shadowing, where individual tree crowns cast

https://doi.org/10.5194/essd-2026-798
Preprint. Discussion started: 22 October 2026
© Author(s) 2026. CC BY 4.0 License.

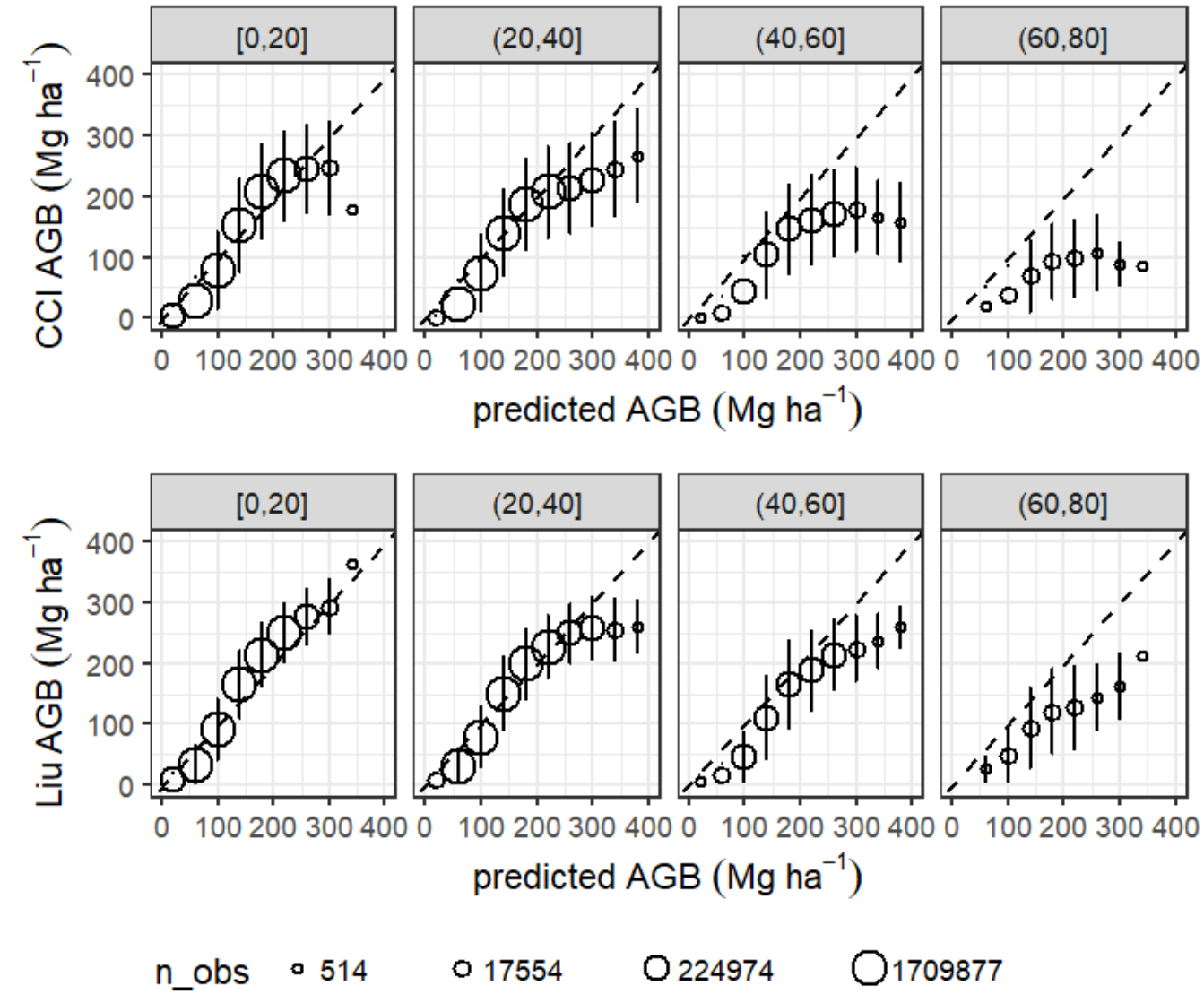


Figure 7: Scatterplots of average and standard deviation Above-Ground Biomass (AGB) from CCI Biomass and Liu per reference range from AGB predicted in this study. The scatterplots are additionally divided into terrain slope class ranges (0-20; 20-40; 40-60; 60-80 °). The dashed line corresponds to the y = x line. If the error bars do not overlap the y = x line then bias is the dominant error in that AGB range. Circles show the mean Above-Ground Biomass (AGB) in

https://doi.org/10.5194/essd-2026-798
Preprint. Discussion started: 22 October 2026
© Author(s) 2026. CC BY 4.0 License.

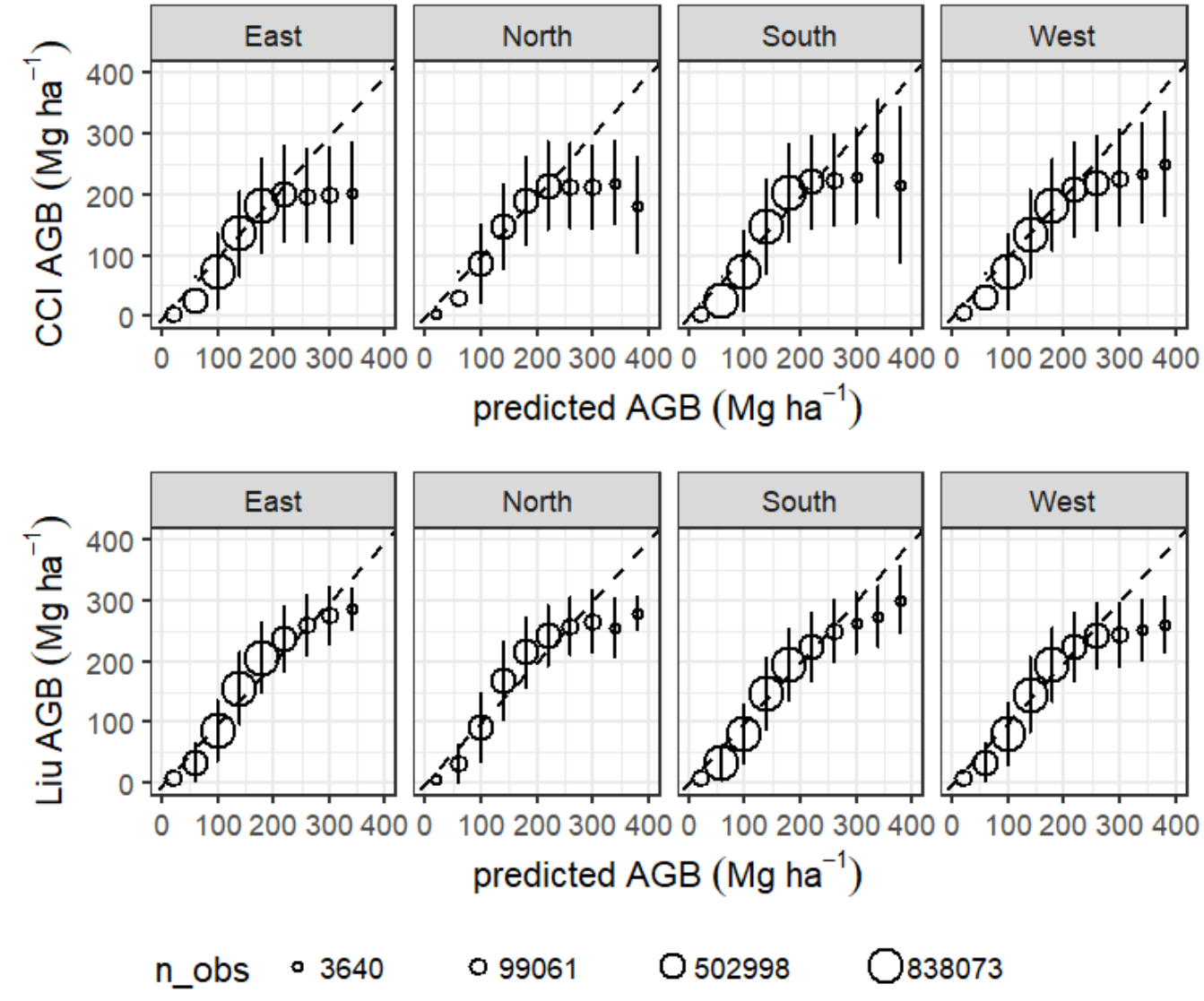


Figure 8: Scatterplots of average and standard deviation Above-Ground Biomass (AGB) from CCI Biomass and Liu per reference range from AGB predicted in this study. The scatterplots are additionally divided into terrain aspect class ranges (East; North; South; West). The dashed line corresponds to the y = x line. If the error bars do not overlap the y = x line then bias is the dominant error in that AGB range. Circles show the mean Above-Ground Biomass (AGB)

https://doi.org/10.5194/essd-2026-798
Preprint. Discussion started: 22 October 2026
© Author(s) 2026. CC BY 4.0 License.



in each 40 Mg ha⁻¹ wide interval of reference AGB. Error metrics and inter-product differences should be interpreted as variations within an uncertainty framework rather than as absolute errors.

365

AGB value ranges were assessed over three distinct landscapes as described in 2.8. The spatial distribution of the biomass appears to have been overall similarly captured by all products in the selected cut-out-areas. For scene i), higher AGB values were found to be concentrated at lower altitudes towards the valley in the center of the scene (Fig. S12), reflecting a clear altitudinal gradient (Fig. 9, column 1). This pattern is consistent among all products. In scene i), median AGB from CCI
370 Biomass was 116 Mg ha⁻¹ (IQR: 82-154), median AGB from Liu of 169 Mg ha⁻¹ (IQR: 109-234) and median predicted AGB of 133 Mg ha⁻¹ (IQR: 83.6-190) (Fig. 10).

Our AGB product seems to capture spatial patterns and possibly forest type variations (Fig. S13) with greater detail, which could be explained by the use of multi-data source embeddings compared to single domain-based products.

Spatial variability of AGB is clearly visible in the predicted product, while CCI Biomass shows a higher degree of homogeneity
375 and negative skewness in scene ii) (Fig. 8, column 2). While RADAR-based AGB estimates at high biomass ranges on steep and north-east oriented slopes showed to suffer from a systematic underestimation (Fig. 7 and 8), geometric distortions can cause localized overestimation depending on the slope's orientation relative to the RADAR sensor. Scene ii) thus revealed higher discrepancies between products with a median CCI AGB of 177 Mg ha⁻¹ (IQR: 118-234), median AGB from Liu of 187 Mg ha⁻¹ (IQR: 125-243) and median predicted AGB of 149 Mg ha⁻¹ (IQR: 108-177). The lower overall AGB values
380 yielded by our product exhibit stronger alignment with the NFI plot-based estimates for European beech forests within the cutout area (median: 57.57, max: 138).

Our product demonstrates high consistency with CCI Biomass in scene iii), regarding both the spatial distribution and range of AGB values, while Liu's product revealed higher degrees of homogeneity and higher AGB values across the landscape (Fig. 9, column 3). Scene iii) revealed a substantial agreement between CCI Biomass and predicted AGB with medians of 82
385 Mg ha⁻¹ (IQR: 65-108) and 75.6 Mg ha⁻¹ (IQR: 63.3-92.1) respectively. AGB from Liu was found to be slightly more negatively skewed with a median AGB of 89 Mg ha⁻¹ (IQR: 68-121).

https://doi.org/10.5194/essd-2026-798
Preprint. Discussion started: 22 October 2026
© Author(s) 2026. CC BY 4.0 License.

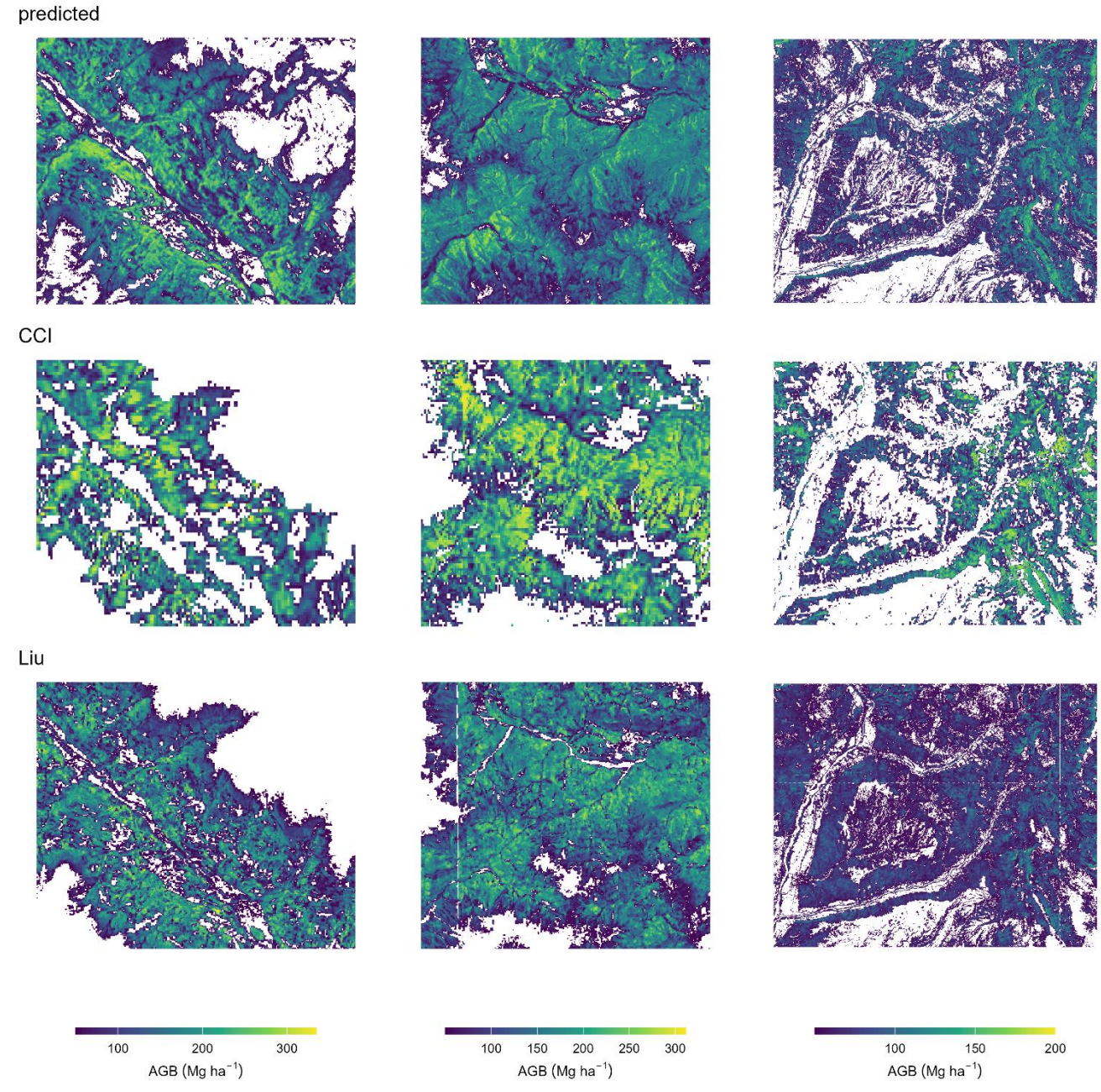


Figure 9: Cut-out areas (approximate size between 0.1x0.1 and 0.2x0.2 degrees) for visual comparison of this study's predicted Above-Ground Biomass (AGB) (Mg ha^{-1}) and CCI Biomass' and Liu's AGB product at their original spatial resolution. The panels in column 1 depict evergreen needleleaf forests (mainly pure Norway spruce stands on moderate to steep exposed slopes (20–60°). In column 2 montane European beech forests with mixed Norway spruce patches on steep terrain (20–70°) are shown. In column 3 a mediterranean oak-dominated forest ecosystem is depicted.

https://doi.org/10.5194/essd-2026-798
Preprint. Discussion started: 22 October 2026
© Author(s) 2026. CC BY 4.0 License.

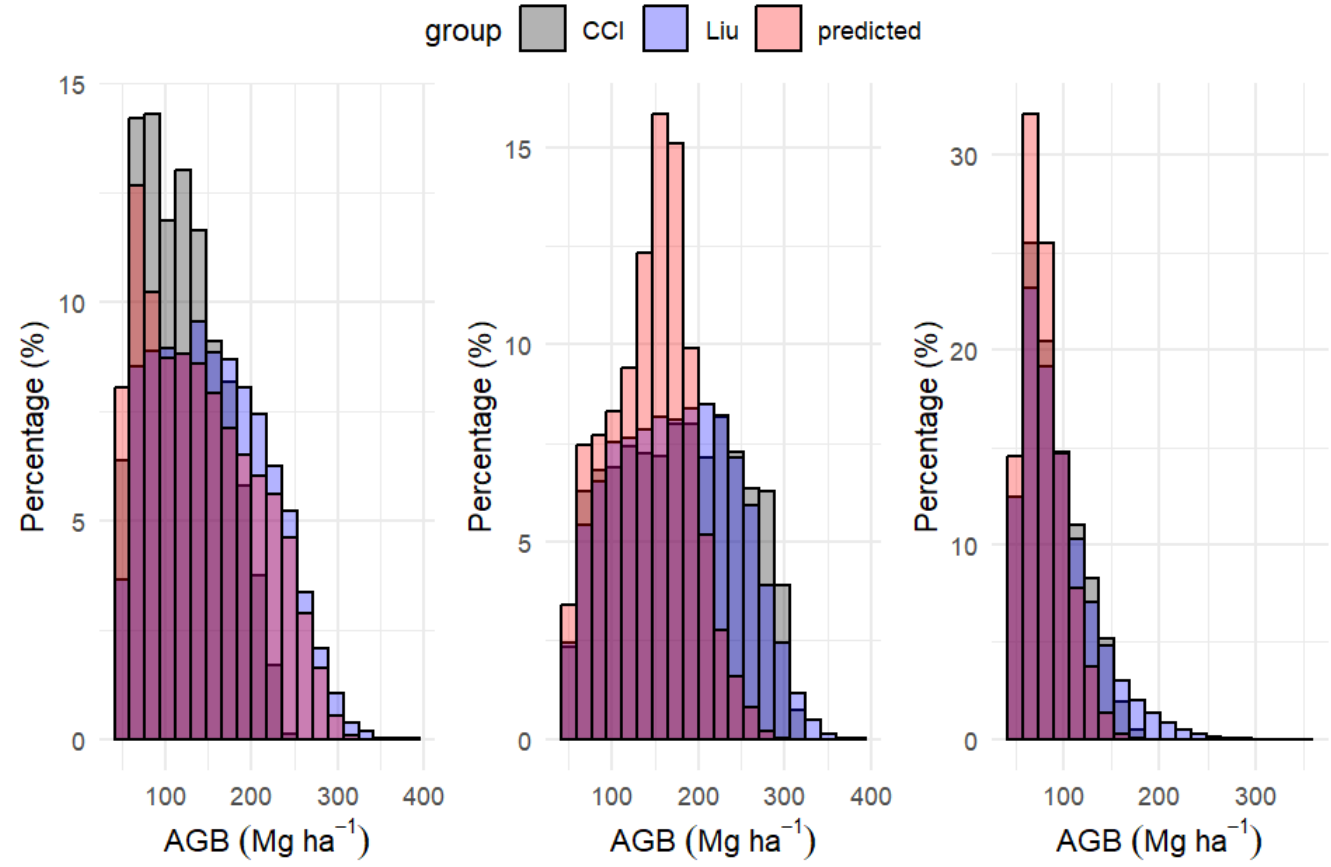


Figure 10: Distribution (%) of Above-Ground Biomass (AGB) (Mg ha^{-1}) for the three cut-out-areas displayed in Figure 9. Subplots are sequenced according to the layout in Figure 9. The AGB distributions for each cut-out-area are grouped by AGB product (CCI, Liu, and predicted; see legend colors).

4 Discussion

Predicting AGB requires simultaneously learning from vegetation greenness, vertical canopy structure, moisture content, and seasonal growth cycles. Unmerged datasets force a model to learn from a single piece of information or to build relationships from disjointed inputs, whereas Satellite Embeddings are provided as vectorized representations of these multi-dimensional biophysical signatures. Because the AEF multi-sensor embeddings fuse different data sources such as optical, thermal, RADAR and meteorological data together through self-supervised learning, the latent space might have superior capacities to establish complex, non-linear relationships between multi-source data, capturing even subtle texture variations and being less sensitive to topographically driven bias. The underlying 64-dimensional feature representation is mathematically structured to

https://doi.org/10.5194/essd-2026-798
Preprint. Discussion started: 22 October 2026
© Author(s) 2026. CC BY 4.0 License.


smooth out localized sensor anomalies and minimize overfitting. Relying entirely on open-access data (AEF Satellite Embeddings and spaceborne GEDI data) rather than local ground measurements, such as NFIs, enables the proposed framework to be easily transferred and scaled across regions. Because the temporal summarization block of the embeddings compresses data relative to specific valid periods, the year of the GEDI observation can be directly matched to the exact corresponding annual embedding layer. This removes seasonal phenological discrepancies from the training target.

Nonetheless, several constraints remain. AEF embeddings are provided as static annual summaries to ensure cloud-free planetary coverage. Therefore, in the case of forest disturbance, the annual embedding might rely heavily on pre-disturbance data from earlier in the year, creating a spatio-temporal mismatch between the structure estimated from GEDI and the time-averaged signal in the embedding. Another limitation is related to the saturation in hyper-dense, multi-layered forests where the passive optical and C-band and L-band RADAR data underpinning AEF potentially still lose their ability to penetrate deep into the lower strata of the canopy. GEDI's direct LiDAR waveform might still capture vertical variations that the 2D-derived embeddings might no longer differentiate.

Spatial alignment might introduce further errors. When pairing a geolocated GEDI pixel with an AEF pixel, GEDI's orbital location uncertainty of around 10-m is propagated with the spatial patch aggregation built into AEF. In highly heterogeneous landscapes, a shift of just a few meters can mean the model is trained on an embedding vector that structurally represents a different canopy patch than the one the GEDI laser registered.

Another limitation concerns the GEDI bias in the lower and higher biomass ranges being propagated into the prediction, compounded by the inability of ensemble decision-tree regressors to extrapolate beyond the truncated boundaries of the training target distributions and by their tendency to optimize towards the mean values.

Considerable uncertainty also persists regarding forest stands on very steep terrain due to a lack of ground data and inherent limitations in spaceborne products. By conducting a comparative analysis, this study quantified the systematic bias built into spaceborne biomass estimations when applied to such complex terrain. At the same time, the majority of the remaining prediction uncertainty persists on steep terrain, as the strict exclusion of training samples on steep slopes restricts the model's empirical exposure. To address these deficiencies in biased areas and unlock yearly updated mapping, future research should explore targeted data selection. Specifically, explicitly including underrepresented tree species or ecoregions in the training dataset, rather than relying on random pixel selection, could significantly improve predictions for local scale analyses.

The provided dataset enables the estimation of carbon stocks and potential sequestration rates, supporting the quantification of the role of forests and other ecosystems in offsetting GHG emissions. By delivering spatially explicit information at high resolution, it also allows for detailed assessment of disturbance impacts (Fig. A4). Annual forest updates are vital to quickly capture the impacts of more frequent environmental threats, including wildfires, extreme weather, and insect outbreaks (Bontemps and Bouriaud, 2024).

Additionally, the dataset further supports applications in environmental and hydrological modelling, given the strong links between vegetation biomass, water fluxes, and energy exchanges within terrestrial ecosystems (Ellison et al., 2017). In this

https://doi.org/10.5194/essd-2026-798
Preprint. Discussion started: 22 October 2026
© Author(s) 2026. CC BY 4.0 License.



context, it can help improve the representation of land surface processes and better constrain modeling frameworks of carbon and water fluxes, contributing to Earth system modeling efforts.

High-resolution AGB estimates reveal local-to-regional product biases in remote and unsampled regions. Analysing how these errors correlate with terrain and forest structure helps identify the drivers of global dataset discrepancies, guiding the development of more accurate retrieval approaches (Araza et al., 2022).

From a policy perspective, the dataset contributes to the provision of baseline statistics for climate policy and strategic planning (Herold et al., 2019). In mountainous regions, its spatial detail enables the identification of variability and hotspot areas, including degraded forests, thereby supporting the prioritization of reforestation and afforestation initiatives.

5 Conclusion

A high-resolution gridded dataset of AGB for the Alpine Convention extent was presented. It was derived by integrating publicly available EO products from different sensor types without relying on field-derived measurements. The dataset allows us to extract and analyze the fine-scale distribution of AGB. This represents a valuable source of spatially continuous information for the alpine region. Besides enabling the estimation of carbon stocks, the dataset facilitates its use for a wide range of applications requiring spatially explicit information at high resolution, such as environmental modeling, hydrological analysis, impact studies, and remote sensing data validation. The presented product is designed to be updated by the next GEDI overpass. This will allow us to respond to more operational purposes such as land cover change and disturbance detection and implications on AGB loss by assessing spatio-temporal variability.

Code and data availability

The dataset and code presented in this work are available in a dedicated repository: https://doi.org/10.5281/zenodo.23073080 (Candotti and Tomelleri, 2026)

The Alpine Convention Perimeter can be downloaded from: https://www.atlas.alpconv.org/#/

GEDI L4A Aboveground Biomass Density v.2.1 data can be accessed at: https://developers.google.com/earthengine/datasets/catalog/LARSE_GEDI_GEDI04_A_002.

Satellite Embedding V1 can be retrieved from: https://developers.google.com/earthengine/datasets/catalog/GOOGLE_SATELLITE_EMBEDDING_V1_ANNUAL 20 435

ESA CCI Above-ground Biomass (v.6) can be accessed from: https://developers.google.com/earthengine/datasets/catalog/ESA_CCI_Above_Ground_Biomass_V6_0?hl=it

Canopy height and biomass from Europe v.0.1 by Liu et al. (2023) is stored under: 10.5281/zenodo.8154444

https://doi.org/10.5194/essd-2026-798
Preprint. Discussion started: 22 October 2026
© Author(s) 2026. CC BY 4.0 License.



Terrain aspect, slope and elevation were retrieved from Copernicus DEM (GLO-30 / GLO-30 Public) available under https://dataspace.copernicus.eu/

E-OBS climate data can be accessed at: 10.24381/cds.151d3ec6

The ForestPaths: European Tree Genus Map is available at: 10.5281/zenodo.13341104

Coordinates of the italian National Forest Inventory (NFI) sample plots used for independent validation are restricted and kept confidential under national data protection and inventory integrity policies. Requests for data access or authorized usage for scientific research can be submitted to the Comando Unità Forestali Ambientali e Agroalimentari (CUFA). Basic inventory data can be downloaded from: https://www.inventarioforestale.org/en/category/servizio-per-laccesso-ai-dati-elementari/

Appendix A

Elevation acts as a critical driver of above-ground biomass (AGB) in alpine ecosystems, primarily by modulating local climatic conditions. The highest AGB variance was found within the lower montane elevation belts (< 1000 m a.s.l.), where AGB accumulation can be driven by a higher tree species richness, a higher plasticity in tree structural traits and historical forest management (Leuschner and Ellenberg, 2017). AGB was found to follow a pyramidal pattern with respect to elevation, peaking specifically in the montane belt (1000–1500 m a.s.l.), possibly due to optimal environmental conditions at mid-altitudes (Fig. A1). This peak coincides with the ideal growing conditions for Norway spruce, a major high-stock species that accumulates substantial biomass in these montane forests (Caudullo et al., 2016). As elevation increases, the harsh environmental gradients, characterized by declining temperatures and shortened growing seasons, typically lead to a pronounced reduction in AGB. At elevations above 1500 and 200 m a.s.l. AGB values decrease rapidly as growing seasons shorten and species composition changes. The predicted median AGB values of 50–100 Mg ha^{-1} align with field-based estimates reported for subalpine forests near the alpine treeline (Rota et al., 2024)

https://doi.org/10.5194/essd-2026-798
Preprint. Discussion started: 22 October 2026
© Author(s) 2026. CC BY 4.0 License.

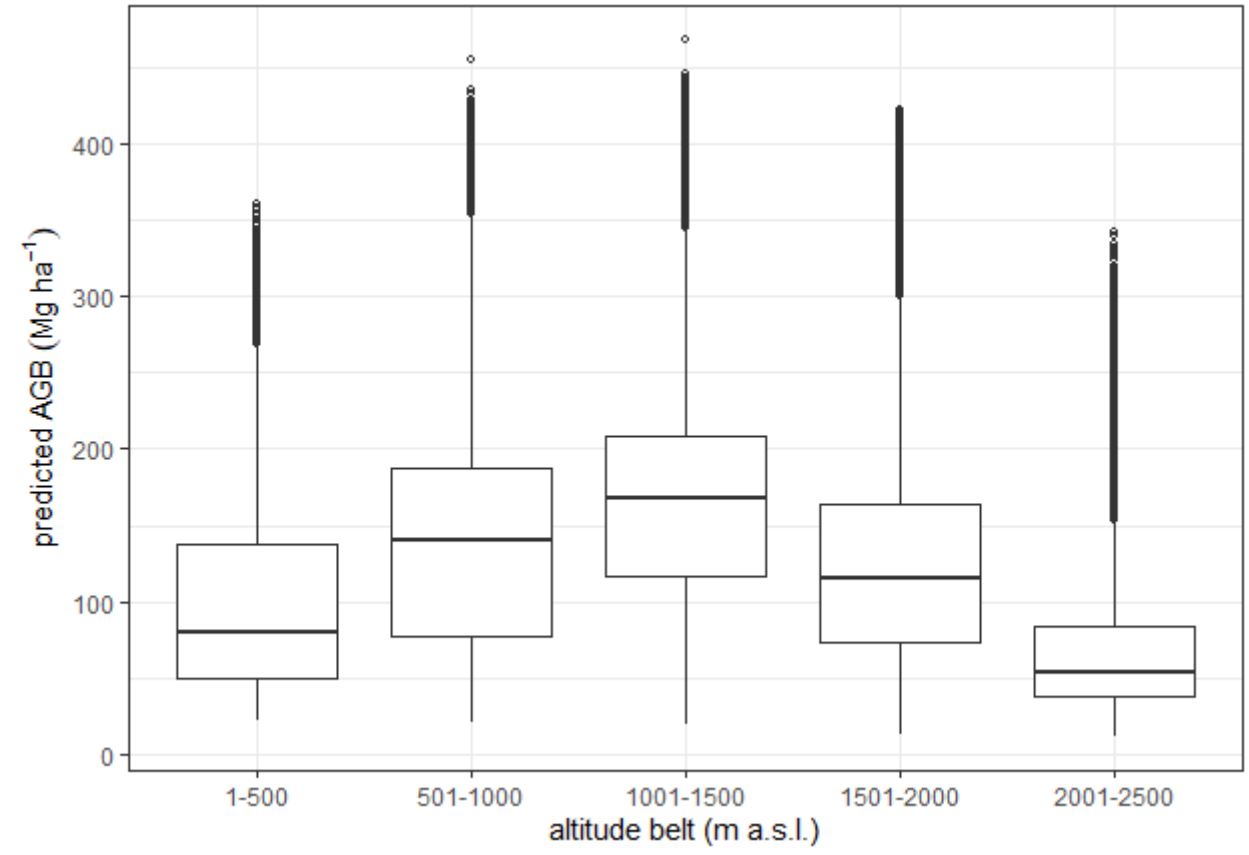


Figure A1: Spatial patterns of above-ground biomass (AGB) (Mg ha^{-1}) by altitude belt in 50 million randomly selected pixels. Elevation above sea-level (m a.s.l.) was binned into five altitude belt classes respectively 1-500, 501-1000, 1001-1500, 1501-2000, 2001-2500 m a.s.l.

Temperature and precipitation are often considered as important factors affecting biomass distribution. Higher temperatures and precipitation promote plant photosynthesis, increasing plant productivity and nutrient accumulation, thereby boosting biomass. Consequently, lower AGB values were consistently found in grid cells with a mean annual temperature below 0 °C, where low temperatures limit metabolic processes. However, in mountain ecosystems, regimes characterized by lower temperatures and higher precipitation can sustain elevated AGB levels (Fig. A2). Lower temperature zones may foster species-specific climatic niches, such as those favoring Norway spruce, a highly productive, high-volume timber species (Caudullo et al., 2016). Due to higher mean annual temperatures (10-15 °C) and limited precipitation (< 1000 mm), Mediterranean

https://doi.org/10.5194/essd-2026-798
Preprint. Discussion started: 22 October 2026
© Author(s) 2026. CC BY 4.0 License.



ecosystems generally exhibit lower AGB accumulation. This trend is driven by species composition, as more arid environments favor slow-growing, drought-tolerant species with lower structural stature and wood volume.

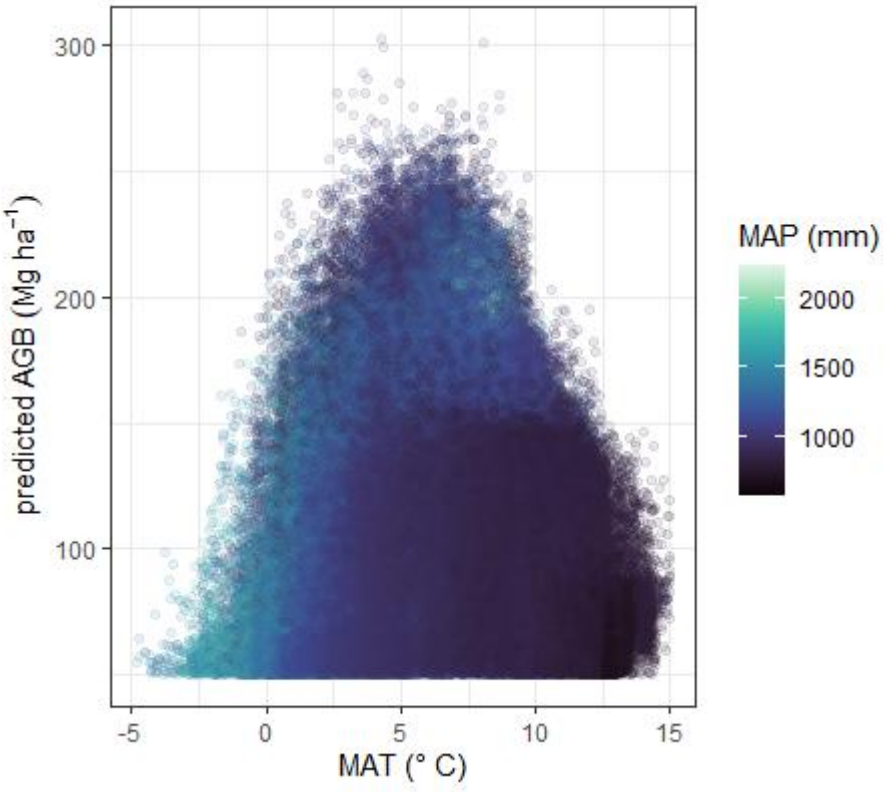


Figure A2: Median above-ground biomass (AGB) (Mg ha⁻¹) by 10x10 km bins as response of mean annual temperature 480 (MAT) (°C) across the alpine range. Values are colored by mean annual precipitation (MAP) (mm). Meteorological variables were retrieved from E-OBS climate data (10.24381/cds.151d3ec6).

The highest AGB estimates were observed in the coniferous tree species (Fig. A3). In the Alps, the trend of higher AGB in coniferous species compared to broadleaved species is strongly driven by elevation zoning and forest management history (Leuschner and Ellenberg, 2017). Historical management created dense, high-volume conifer monocultures that artificially inflated localized conifer AGB metrics relative to surrounding mixed or deciduous stands. Additionally, conifers possess a narrow, conical geometry allowing tighter stand packaging. This structural setup allows a higher number of large-diameter trees per hectare compared to branching broadleaved canopies. Due to exceptionally dense, multi-layered stands and its ecological optimum in the humid and well-drained montane belts of the eastern Alps, also European beech can be characterized by high AGB. The reduction of AGB in broadleaved species, which are predominant in the western Alps, was explained due to more persistent droughts and shallow, rocky soils that constrain vertical tree growth (Vallet and Mouillot, 2026).

https://doi.org/10.5194/essd-2026-798
Preprint. Discussion started: 22 October 2026
© Author(s) 2026. CC BY 4.0 License.

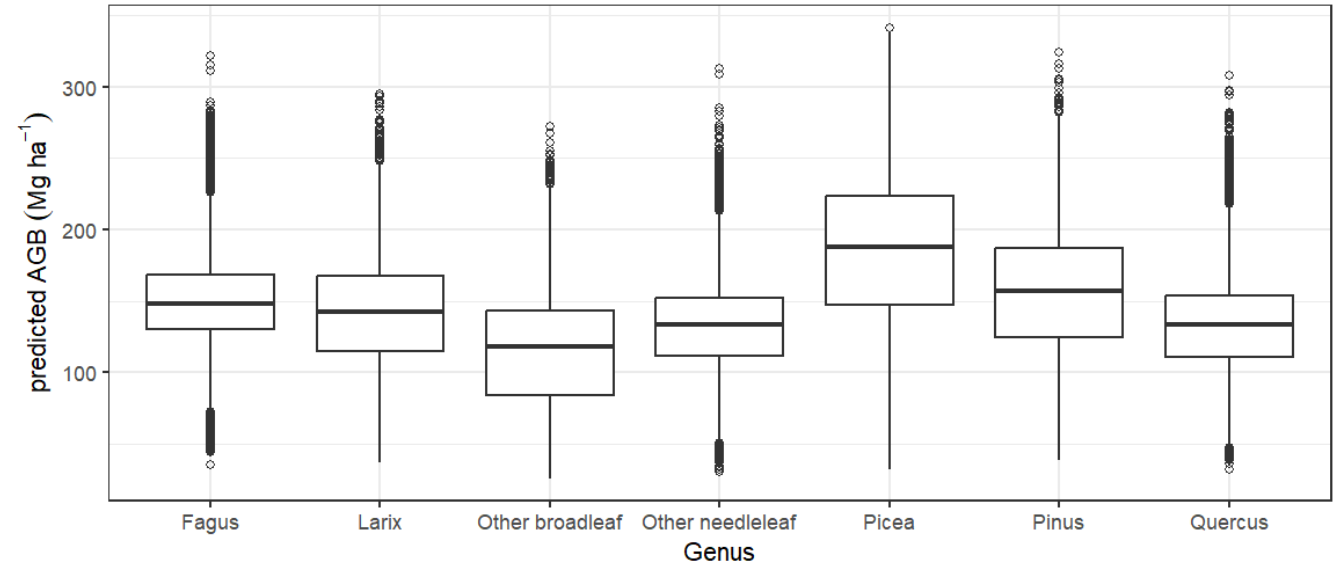


Figure A3: Above-ground biomass (AGB) (Mg ha^{-1}) by forest genus from the Forest Path European tree genus map (10.5281/zenodo.13341104). Distributions were derived from 50 million randomly selected pixels.

A cross-product comparison revealed distinct AGB distribution patterns when comparing AGB loss induced by a severe windstorm event that hit the Southern Alps in 2018 to the intact reference forest. In the predicted product of this study, the intact forest baseline exhibited a median AGB of 153.3 Mg ha−1, which dropped to 66 Mg ha−1 within the wind disturbed areas, representing a relative median change of 57%. In comparison, the global ESA CCI dataset captured a baseline median of 148.5 Mg ha−1 and a post-disturbance median of 105.2 Mg ha−1 (29.1% change). The Liu product tracked a baseline median of 165 Mg ha−1 and a disturbed median of 112 Mg ha−1, indicating a relative shift of 32 %. The probability density distributions highlight varying sensitivities among the products, with the predicted dataset providing a more pronounced separation between disturbed and intact forest, compared to the other two products.

https://doi.org/10.5194/essd-2026-798
Preprint. Discussion started: 22 October 2026
© Author(s) 2026. CC BY 4.0 License.

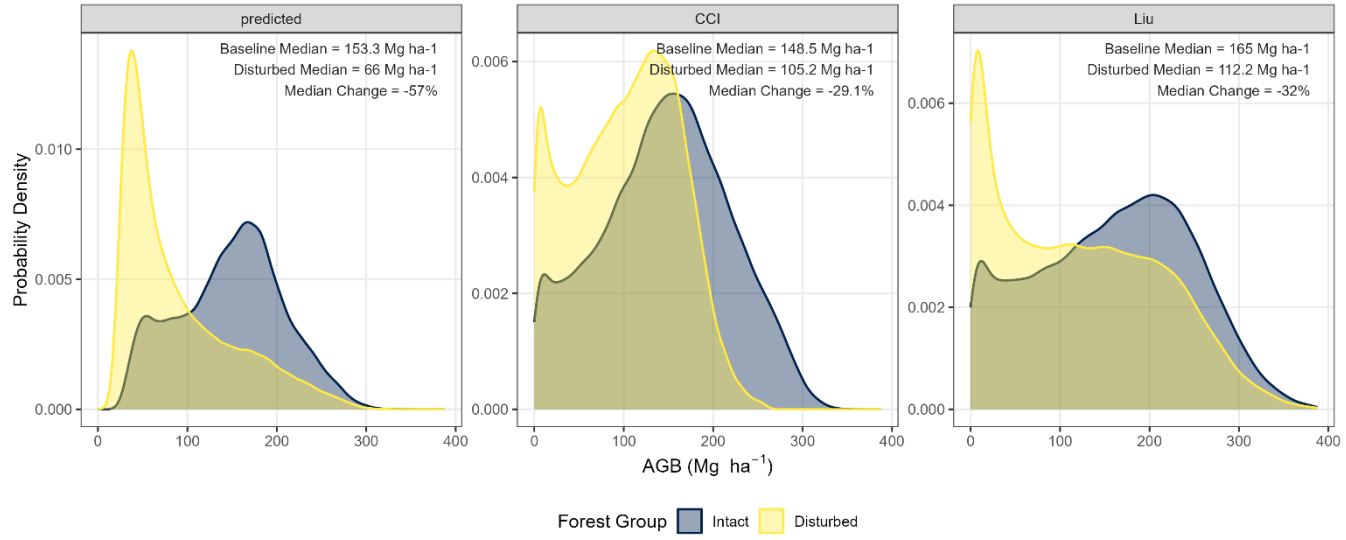


Figure A4: Probability density distributions of Above-Ground Biomass (AGB; Mg ha^{-1}) across wind-disturbed forest patches (Vaia windstorm 2018, yellow) and adjacent intact forest control baselines (dark blue). Disturbed cores were isolated via a 2-pixel inward erosion, while control intact forest baselines were extracted from an outer ring buffer of 2 to 4 pixels, strictly restricted to forest land cover classes using the ESA CCI Land Cover mask. Panels show the predicted AGB against CCI and Liu AGB datasets. Inset panels display the baseline intact forest median, disturbed forest median, and the relative percentage change.

https://doi.org/10.5194/essd-2026-798
Preprint. Discussion started: 22 October 2026
© Author(s) 2026. CC BY 4.0 License.



Author contributions

The study was conceptualized by AC. AC processed and analysed the data, created figures and wrote the original draft. ET provided funding and supervision. Both authors reviewed, discussed, revised and approved the final draft.

Competing interests

The authors declare that they have no conflict of interest.

Disclaimer

Copernicus Publications remains neutral with regard to jurisdictional claims made in the text, published maps, institutional affiliations, or any other geographical representation in this paper. While Copernicus Publications makes every effort to include appropriate place names, the final responsibility lies with the authors. Views expressed in the text are those of the authors and do not necessarily reflect the views of the publisher. Neither the European Commission nor ECMWF is responsible for any use that may be made of the Copernicus information or data it contains.

Acknowledgements

We extend our sincere gratitude to Maurizio Santoro for his valuable advice and critical feedback during the preparation of this manuscript.

Financial support

This work was supported by the Cohesion Italy 21-27 Project EFRE1079 “Forest Robotic Monitoring and Automation (FORMA)”, co-funded by the EU and the Autonomous Province of Bozen-Bolzano.

https://doi.org/10.5194/essd-2026-798
Preprint. Discussion started: 22 October 2026
© Author(s) 2026. CC BY 4.0 License.



References

Araza, A., de Bruin, S., Herold, M., Quegan, S., Labriere, N., Rodriguez-Veiga, P., Avitabile, V., Santoro, M., Mitchard, E. T. A., Ryan, C. M., Phillips, O. L., Willcock, S., Verbeeck, H., Carreiras, J., Hein, L., Schelhaas, M. J., Pacheco-Pascagaza, A. M., da Conceição Bispo, P., Laurin, G. V., Vieilledent, G., Slik, F., Wijaya, A., Lewis, S. L., Morel, A., Liang, J., Sukhdeo, H., Schepaschenko, D., Cavlovic, J., Gilani, H., and Lucas, R.: A comprehensive framework for assessing the accuracy and uncertainty of global above-ground biomass maps, Remote Sens. Environ., 272, https://doi.org/10.1016/j.rse.2022.112917, 2022.

Avitabile, V. and Camia, A.: An assessment of forest biomass maps in Europe using harmonized national statistics and inventory plots, For. Ecol. Manage., 409, 489–498, https://doi.org/10.1016/j.foreco.2017.11.047, 2018.

Baccini, A., Laporte, N., Goetz, S. J., Sun, M., and Dong, H.: A first map of tropical Africa's above-ground biomass derived from satellite imagery, Environmental Research Letters, 3, https://doi.org/10.1088/1748-9326/3/4/045011, 2008.

Baccini, A., Goetz, S. J., Walker, W. S., Laporte, N. T., Sun, M., Sulla-Menashe, D., Hackler, J., Beck, P. S. A., Dubayah, R., Friedl, M. A., Samanta, S., and Houghton, R. A.: Estimated carbon dioxide emissions from tropical deforestation improved by carbon-density maps, Nat. Clim. Chang., 2, 182–185, https://doi.org/10.1038/nclimate1354, 2012.

Beck, J., B. Wirt, J. Armston, M. Hofton, S. Luthcke, and H. Tang. 2021. "Global Ecosystem Dynamics Investigation (GEDI) Level 02 User Guide." *Land Processes Distributed Active Archive Center (DAAC)*, *April*.https://lpdaac.usgs.gov/documents/988/GEDI02_User_Guide_V2.pdf

Belgiu, M. and Drăgu, L.: Random forest in remote sensing: A review of applications and future directions, https://doi.org/10.1016/j.isprsjprs.2016.01.011, 1 April 2016.

Bontemps, J. D. and Bouriaud, O.: Take five: about the beat and the bar of annual and 5-year periodic national forest inventories, https://doi.org/10.1186/s13595-024-01268-1, 1 December 2024.

Brandt, M., Wigneron, J. P., Chave, J., Tagesson, T., Penuelas, J., Ciais, P., Rasmussen, K., Tian, F., Mbow, C., Al-Yaari, A., Rodriguez-Fernandez, N., Schurgers, G., Zhang, W., Chang, J., Kerr, Y., Verger, A., Tucker, C., Mialon, A., Rasmussen, L. V., Fan, L., and Fensholt, R.: Satellite passive microwaves reveal recent climate-induced carbon losses in African drylands, Nat. Ecol. Evol., 2, 827–835, https://doi.org/10.1038/s41559-018-0530-6, 2018.

https://doi.org/10.5194/essd-2026-798
Preprint. Discussion started: 22 October 2026
© Author(s) 2026. CC BY 4.0 License.



595 Brown, C. F., Kazmierski, M. R., Pasquarella, V. J., Rucklidge, W. J., Samsikova, M., Zhang, C., Shelhamer, E., Lahera, E., Wiles, O., Ilyushchenko, S., Gorelick, N., Zhang, L. L., Alj, S., Schechter, E., Askay, S., Guinan, O., Moore, R., Boukouvalas, A., and Kohli, P.: AlphaEarth Foundations: An embedding field model for accurate and efficient global mapping from sparse label data, 2025.

600 Candotti, A., Tomelleri, E. (2026). High-Resolution Above-Ground Biomass Mapping of the Alps using Satellite Embeddings and GEDI [Dataset]. Zenodo. https://doi.org/10.5281/zenodo.23073080

Caudullo, G., Tinner, W., and de Rigo, D. Picea abies in Europe: distribution, habitat, usage and threats. in European atlas of forest tree species. J. San-Miguel-Ayanz, RigoD. de, G. Caudullo, T. Houston Durrant and A. Mauri Luxembourg: European
605 Union, e012300. 2016.

Cornes, R. C., van der Schrier, G., van den Besselaar, E. J. M., and Jones, P. D.: An Ensemble Version of the E-OBS Temperature and Precipitation Data Sets, Journal of Geophysical Research: Atmospheres, 123, 9391–9409, https://doi.org/10.1029/2017JD028200, 2018.

610

Dubayah, R., Blair, J. B., Goetz, S., Fatoyinbo, L., Hansen, M., Healey, S., Hofton, M., Hurtt, G., Kellner, J., Luthcke, S., Armston, J., Tang, H., Duncanson, L., Hancock, S., Jantz, P., Marselis, S., Patterson, P. L., Qi, W., & Silva, C. The Global Ecosystem Dynamics Investigation: High-resolution laser ranging of the Earth's forests and topography. *Science of Remote Sensing*100002. 10.1016/j.srs.2020.100002. 2020.

615

Dubayah, R., Armston, J., Healey, S. P., Bruening, JM., Patterson, P. L., Kellner, J. R., Duncanson, L., Saarela, S., Ståhl, G., Yang, Z., Tang, H., Blair, J. B., Fatoyinbo, L., Goetz, S., Hancock, S., Hansen, M., Hofton, M., Hurtt, G., & Luthcke, S. GEDI launches a new era of biomass inference from space. *Environmental Research Letters*, *17*(9), 095001. 2022.

620 Ellison, D., Morris, C. E., Locatelli, B., Sheil, D., Cohen, J., Murdiyarso, D., Gutierrez, V., Noordwijk, M. van, Creed, I. F., Pokorny, J., Gaveau, D., Spracklen, D. V., Tobella, A. B., Ilstedt, U., Teuling, A. J., Gebrehiwot, S. G., Sands, D. C., Muys, B., Verbist, B., Springgay, E., Sugandi, Y., and Sullivan, C. A.: Trees, forests and water: Cool insights for a hot world, Global Environmental Change, 43, 51–61, https://doi.org/10.1016/j.gloenvcha.2017.01.002, 2017.

625 Fan, L., Wigneron, J. P., Ciais, P., Chave, J., Brandt, M., Fensholt, R., Saatchi, S. S., Bastos, A., Al-Yaari, A., Hufkens, K., Qin, Y., Xiao, X., Chen, C., Myneni, R. B., Fernandez-Moran, R., Mialon, A., Rodriguez-Fernandez, N. J., Kerr, Y., Tian, F.,

© Author(s) 2026. CC BY 4.0 License.



and Peñuelas, J.: Satellite-observed pantropical carbon dynamics, https://doi.org/10.1038/s41477-019-0478-9, 1 September 2019.

Fattorini, L., Marcheselli, M., and Pisani, C.: A three-phase sampling strategy for large-scale multiresource forest inventories, J. Agric. Biol. Environ. Stat., 11, 296–316, https://doi.org/10.1198/108571106X130548, 2006.

Harris, N. L., Gibbs, D. A., Baccini, A., Birdsey, R. A., de Bruin, S., Farina, M., Fatoyinbo, L., Hansen, M. C., Herold, M., Houghton, R. A., Potapov, P. V., Suarez, D. R., Roman-Cuesta, R. M., Saatchi, S. S., Slay, C. M., Turubanova, S. A., and Tyukavina, A.: Global maps of twenty-first century forest carbon fluxes, Nat. Clim. Chang., 11, 234–240, https://doi.org/10.1038/s41558-020-00976-6, 2021.

Herold, M., Carter, S., Avitabile, V., Espejo, A. B., Jonckheere, I., Lucas, R., McRoberts, R. E., Næsset, E., Nightingale, J., Petersen, R., Reiche, J., Romijn, E., Rosenqvist, A., Rozendaal, D. M. A., Seifert, F. M., Sanz, M. J., and De Sy, V.: The Role and Need for Space-Based Forest Biomass-Related Measurements in Environmental Management and Policy, https://doi.org/10.1007/s10712-019-09510-6, 15 July 2019.

De Keersmaecker, W., Zanaga, D., Senf, C., Viana-Soto, A., Klapper, J., Blickensdörfer, L., Govaere, L., Lerink, B., Leyman, A., Schelhaas, M.-J., Teeuwen, S., Verkerk, P. J., and Van De Kerchove, R.: ForestPaths: European tree genus map, https://doi.org/10.5281/zenodo.13341104, August 2024.

Kellner, J. R., Armston, J., and Duncanson, L.: Algorithm Theoretical Basis Document for GEDI Footprint Aboveground Biomass Density, Earth and Space Science, 10, https://doi.org/10.1029/2022EA002516, 2023.

Klaas-Witt, T. and Emeis, S.: The five main influencing factors for lidar errors in complex terrain, Wind Energy Science, 7, 413–431, https://doi.org/10.5194/wes-7-413-2022, 2022.

Leuschner, C., and Ellenberg, H. Abiotic conditions, flora, ecosystem functions and recent human influence. in Ecology of Central European forests: vegetation ecology of Central Europe. eds. C. Leuschner and H. Ellenberg (Cham: Springer International Publishing). 2017.

Liu, S., Brandt, M., Nord-Larsen, T., Chave, J., Reiner, F., Lang, N., Tong, X., Ciais, P., Igel, C., Pascual, A., Guerra-Hernandez, J., Li, S., Mugabowindekwe, M., Saatchi, S., Yue, Y., Chen, Z., and Fensholt, R.: E C O LO G Y The overlooked contribution of trees outside forests to tree cover and woody biomass across Europe, 2023.

https://doi.org/10.5194/essd-2026-798
Preprint. Discussion started: 22 October 2026
© Author(s) 2026. CC BY 4.0 License.



Pan, Y., Birdsey, R. A., Phillips, O. L., and Jackson, R. B.: The structure, distribution, and biomass of the world's forests, https://doi.org/10.1146/annurev-ecolsys-110512-135914, 2013.

Rodríguez-Veiga, P., Quegan, S., Carreiras, J., Persson, H. J., Fransson, J. E. S., Hoscilo, A., Ziółkowski, D., Stereńczak, K., Lohberger, S., Stängel, M., Berninger, A., Siegert, F., Avitabile, V., Herold, M., Mermoz, S., Bouvet, A., Le Toan, T., Carvalhais, N., Santoro, M., Cartus, O., Rauste, Y., Mathieu, R., Asner, G. P., Thiel, C., Pathe, C., Schmullius, C., Seifert, F. M., Tansey, K., and Balzter, H.: Forest biomass retrieval approaches from earth observation in different biomes, International Journal of Applied Earth Observation and Geoinformation, 77, 53–68, https://doi.org/10.1016/j.jag.2018.12.008, 2019.

Rota, N., Canedoli, C., Ferré, C., Comolli, R., Abu El Khair, D., and Padoa-Schioppa, E.: Assessing the carbon stock in the Alps: Considerations on three different approaches, J. Nat. Conserv., 82, https://doi.org/10.1016/j.jnc.2024.126746, 2024.

Saatchi, S. S., Harris, N. L., Brown, S., Lefsky, M., Mitchard, E. T. A., Salas, W., Zutta, B. R., Buermann, W., Lewis, S. L., Hagen, S., Petrova, S., White, L., Silman, M., and Morel, A.: Benchmark map of forest carbon stocks in tropical regions across three continents, Proc. Natl. Acad. Sci. U. S. A., 108, 9899–9904, https://doi.org/10.1073/pnas.1019576108, 2011.

Salazar-Neira, J. C., Mialon, A., Richaume, P., Mermoz, S., Kerr, Y. H., Bouvet, A., Le Toan, T., Boitard, S., and Rodriguez-Fernandez, N. J.: Above-Ground Biomass Estimation Based on Multi-Angular L-Band Measurements of Brightness Temperatures, IEEE J. Sel. Top. Appl. Earth Obs. Remote Sens., 16, 5813–5827, https://doi.org/10.1109/JSTARS.2023.3285288, 2023.

Santoro, M., Cartus, O., Carvalhais, N., Rozendaal, D. M. A., Avitabile, V., Araza, A., De Bruin, S., Herold, M., Quegan, S., Rodríguez-Veiga, P., Balzter, H., Carreiras, J., Schepaschenko, D., Korets, M., Shimada, M., Itoh, T., Moreno Martínez, Á., Cavlovic, J., Gatti, R. C., Da Conceição Bispo, P., Dewnath, N., Labrière, N., Liang, J., Lindsell, J., Mitchard, E. T. A., Morel, A., Pacheco Pascagaza, A. M., Ryan, C. M., Slik, F., Vaglio Laurin, G., Verbeeck, H., Wijaya, A., and Willcock, S.: The global forest above-ground biomass pool for 2010 estimated from high-resolution satellite observations, Earth Syst. Sci. Data, 13, 3927–3950, https://doi.org/10.5194/essd-13-3927-2021, 2021.

Schwartz, M., Ciais, P., De Truchis, A., Chave, J., Ottlé, C., Vega, C., Wigneron, J. P., Nicolas, M., Jouaber, S., Liu, S., Brandt, M., and Fayad, I.: FORMS: Forest Multiple Source height, wood volume, and biomass maps in France at 10 to 30 m resolution based on Sentinel-1, Sentinel-2, and Global Ecosystem Dynamics Investigation (GEDI) data with a deep learning approach, Earth Syst. Sci. Data, 15, 4927–4945, https://doi.org/10.5194/essd-15-4927-2023, 2023.

https://doi.org/10.5194/essd-2026-798
Preprint. Discussion started: 22 October 2026
© Author(s) 2026. CC BY 4.0 License.



Shendryk, Y.: Fusing GEDI with earth observation data for large area aboveground biomass mapping, https://doi.org/10.1016/j.jag.2022.103108, 1 December 2022.

Tabacchi, G., L. Di Cosmo, P. Gasparini, and S. Morelli. 2011. Stima del volume e della fitomassa delle principali specie forestali italiane 75–88. Trento: Consiglio per la Ricerca e la sperimentazione in Agricoltura, Unità di Ricerca per il Monitoraggio e la Pianificazione Forestale.

Tomppo, E., Gschwantner, T., Lawrence, M., and Mcroberts, R. E.: National Forest Inventories Pathways for Common Reporting A B 3, 2010.

Vallet, L. and Mouillot, F.: How climate, fire types and topography drive forest biomass vulnerability to fires assessed from high resolution space-for-time analysis, Ecol. Indic., 186, https://doi.org/10.1016/j.ecolind.2026.114850, 2026.